Arjun Singh, Vitaly Petrov, Priyangshu Sen, and Josep Miquel Jornet

Near-Field Terahertz Communications for 6G and Beyond

From concepts to realizations

©SHUTTERSTOCK.COM/LEON_PHOTOGRAPHY

Digital Object Identifier 10.1109/MSP.2024.3496395
Date of current version: 13 March 2025

The terahertz (THz) band (0.3–3 THz) has gained widespread attention from the scientific community over the past decade for wireless sensing and communications. Initially, from believing that the THz band couldn't really be exploited beyond some necessary sensing for Earth exploration and radio astronomy, the consensus among the research community is now shifting to where it is considered that THz, and even more significantly, sub-THz (100–300-GHz) bands will form the basis of 6G and future generations of wireless communications as well as enabling next-generation sensing capabilities.

Introduction

The first wave of research exploring THz communications was mainly concentrated in two major directions: 1) revealing the principal tradeoffs involved in THz communications and characterizing the THz-specific effects, such as atmospheric absorption, and 2) developing THz devices. With developments relating to device technology, new waveform modulations, signal processing techniques, and robust digital back ends, the so-called "THz technology gap" is slowly closing [1]. As such, point-to-point THz links have been demonstrated as well as the first standard on THz wireless. The next step is to focus on advancing THz communications by enabling mobility. Mobile here refers not just to angular but also to distance-dependent movement. However, mobile links that utilize the THz band require a unique evaluation to properly design the full communication stack that addresses link and system-level challenges related to end-to-end connectivity, reliability, mobility support, and energy efficiency. Unlike the prior legacy wireless counterparts, the large electrical aperture of THz devices forces researchers to work in the THz near-field, a new "no man's land" for wireless commercial networks of the past or present. This introduces new challenges and opportunities.

A brief history of THz communications, near-field signal processing, and their rendezvous

Initially, THz communications were mainly considered for small-scale nanonetworks, sensing-based applications, and

broader goals of Earth exploration and radio astronomy, in which THz signals and the absorption spectrum play a key role [1]. However, as device developments in the THz band were initiated, and work on channel modeling in this region of the spectrum increased, it was seen that, despite the devastating path losses, the absorption losses were mainly restricted to a few absorption spectra. Thus, the band provided an untapped opportunity for enabling next-generation wireless, unhindered by the contention and congestion of a multitude of devices in conventional radio-frequency (RF) bands.

In parallel, near-field phenomena and signal processing have been studied, applied, and utilized for several decades. This extends from RF identification (RFID) tagging to optical sensing and imaging [2]. Indeed, many of the most exciting opportunities and seminal works on near-field beam generation and detection come from the optical regime, with an emphasis on particle manipulation, increased depth of focus, and ultraprecise imaging and sensing [3], [4], [5]. In part, this has been possible since devices that work in the optical regime have been available for a long time because of the breakthrough of laser technology. Near-field signal processing with arrays has also been utilized in distributed beamforming concepts [6].

In enabling THz communications, we see a special convergence of the two fields. Namely, utilizing concepts of near-field processing and beam design in enabling ultrabroadband communications is a novel and unprecedented field. Unsurprisingly, there are several research groups focusing on this aspect [7], [8], [9]. We first see that metasurface-based devices and 3D-printed lenses, which allow the required phases of near-field beams to be implemented, have been proposed, developed, and demonstrated [1]. In addition, work utilizing unconventional beams and seeing how their properties can be utilized or are limited in the THz near field has also been performed [7], [9], [10]. We have now gone from considering THz systems that could conceivably only be imagined in the nanoscale and near-field communications that were somewhat limited to menial tasks, such as RFID tagging, to a place where indoor wireless, small-scale cellular, and advanced Internet of Things communications could all utilize near-field theory. Thus, THz communications have seen the utilization of theory developed in the optical regime to solve problems of the conventional RF regime with physics and channel behavior in the THz domain.

Beamshaping in the THz near field

It may seem contradictory to realize that a larger frequency can lead to an increase in the near field since we always imagine that larger frequencies lead to a smaller size antenna. The difference, however, is that *the same physical size antenna with a larger frequency leads to a larger near-field region*. Taking this observation to the extreme, for example, we would observe that a dipole antenna of an infinitesimally high frequency would have a vanishing size. However, for any practical-size antenna, the near-field distance for this infinitely high frequency would also extend to infinity. Thus, THz devices that provide the nominal gain required to enable communication over meaningful distances (more than a few centimeters) have a large near-field zone, which, for a device with the largest dimension D is given as $2D^2/\lambda$, where λ is the signal wavelength. For example, the near field of a 20-cm antenna array at 120 GHz extends to 32 m. The near field of the same antenna size at 1.05 THz (i.e., the center frequency of the first absorption-defined transmission window above 1 THz) goes to 280 m. If instead a much larger antenna structure, such as a 2-m dish or surface, is used, the near field of this wireless system at 120 GHz and 1.05 THz extends to 3.2 km and 28 km, respectively. This is true irrespective of whether we design the aperture through arrays (still in development for such large scales) or with commercially available horn lens antennas and Cassegrain reflector systems. This becomes even more relevant when we consider intelligent reflecting surfaces (IRSs), one of the breakthrough technologies for THz in 6G in which the aperture size can be scaled significantly. It is important to note that the issue of the near field is present irrespective of whether the radiating aperture is an array or an aperture antenna, such as the current commercially available horn lens or dish antennas, as evidenced in [11].

Traditional communication strategies in the near field, where the signal is assumed to propagate with the plane-wave assumption (uniform phase and where the spreading effect results in a Gaussian intensity [12]), lead to significant challenges. First, the gain of THz devices in the near field is quickly saturated, reducing the energy efficiency of the system tremendously. In addition, the traditional beam-management strategies, including those proposed for THz systems, become inaccurate [10] as the signal is no longer a pencil-thin beam.

At the same time, operating in the THz near field allows us to exploit the prospect of beamshaping. Here, we observe that the properties of a beam generated from an aperture are completely defined by the phase and, in some cases, the amplitude distribution of the electric field at the aperture itself [13]. Thus, the knowledge of the wavefront, i.e., the imaginary line that connects all of the points of a wave with the same phase, is enough to completely characterize the beam [13]. In some cases, the wavefront can be represented as a response of the wireless channel. In this case, we assume the antenna to be omnidirectional, radiating out in all directions. We specifically refer to the electromagnetic (EM) response at the transmitter, which decides how the signal will be radiated. Recent works involving near-field THz have strongly focused on spherical wavefronts. However, nonspherical wavefronts are also possible within the near field. Specifically, in addition to plane-wave canonical beamforming and spherical-wave canonical beamfocusing, we can generate, propagate, and receive exotic beams that have previously never been used in widespread cellular networks [10]. The proper utilization of such beams can provide untapped opportunities for realizing mobile THz links in the dense wireless jungle of the future, taking us down a path of communication that evolves from 5G to 6G and beyond, a vision of which is presented in Figure 1. For example, THz Bessel beams are self-healing and nondiffracting beams that can provide very high signal-to-noise ratio (SNR) links compared to traditional beamforming and

maintain resilient links even against significant blockage—a common problem in directional communications as in the THz domain [14]. Alternatively, Airy-like beams can be utilized for nonline-of-sight (NLOS) links or can bend around corners, even without external resources, such as IRSs [14], thanks to their curving trajectory. Beamfocusing can help in maximum energy efficiency in static configurations by focusing all of the signal energy at a specific spot [8].

Designing efficient near-field THz wireless

The open question that remains is how practical near-field THz-band communication systems can be designed that deliver on the promises of the next generations of wireless networks, which are tentatively marked as having a 1 terabit/s data rate, 0.1-ms latency, and "10^{-9}" reliability [1].

Here, we understand that the final bottleneck is the system capacity, which depends on 1) the available bandwidth, 2) the received SNR, and 3) the spatial reuse factor. While the THz band boasts ample bandwidth, it is accompanied by a substantial increase in noise power, presenting a considerable challenge. Also, the small wavelengths at THz frequencies result in devastating path losses, and further, THz signals are easily obstructed by everyday objects, leading to link breakage. As if that is not enough, the THz channel is also low rank, reducing the channel gains from multiple-input, multiple-output (MIMO) links [15]. These problems must then be tackled within the near field and are already the subjects of study of several significant research groups [1], [8], [10], [16], [17].

Scope and outline of the tutorial

Adapting THz research for efficient wireless systems requires reevaluating propagation models, physical layer designs, and networking solutions inherited from 2G–5G wireless networks. Recent years have seen progress in near-field-specific models, tools, and solutions for mobile THz communications. Accordingly, this article aims to provide an updated look at the field of THz applications for 6G and beyond, while 1) filling knowledge gaps for a coherent understanding of near-field propagation, 2) showcasing some solutions to the envisioned problems, and 3) highlighting the emerging critical challenges and opportunities.

The manuscript provides an updated look at the present state of the art in physical layer development and propagation in near-field THz wireless communications. Significant attention is given to several research groups, especially seminal works. When possible, the discussion is presented to emphasize key concepts, rather than delving into extensive mathematical derivations. However, attention is taken to ensure that the discussion is clear and to the point, with an attempt to make a layman also understand the core concepts. Equations are employed when they are deemed to elucidate a concept more effectively than a detailed discussion, with a greater emphasis on simpler equations over more convoluted ones. While the majority of the discussion is centered on Cartesian coordinates, in various situations rotational symmetry is exploited by emphasizing the cylindrical coordinate system. This change is always emphasized to avoid confusion and only utilized to make the discussion more streamlined.

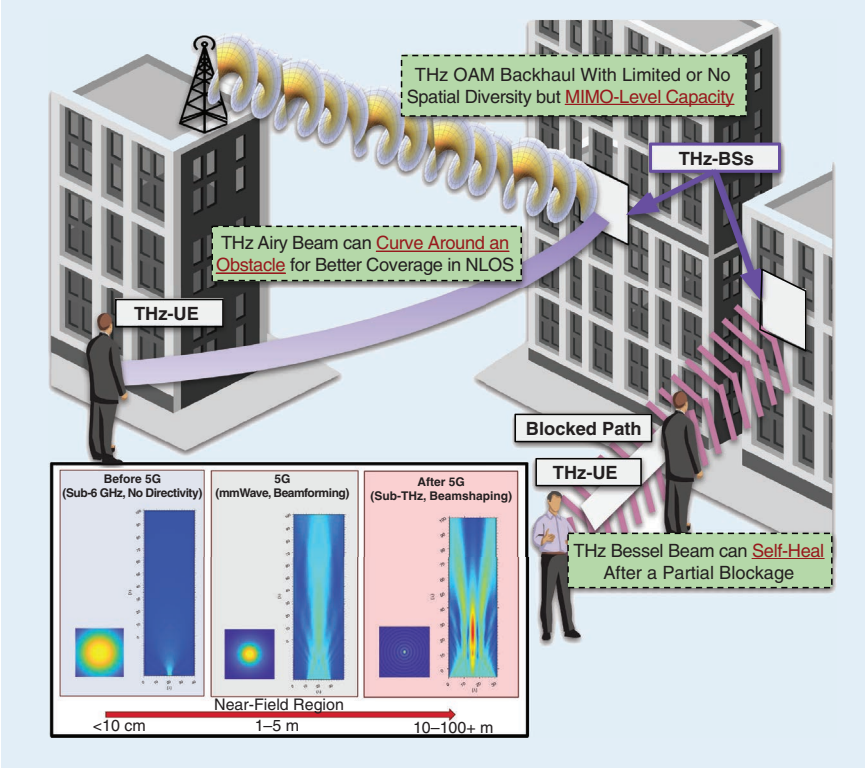

FIGURE 1. Envisioned key novel features introduced by near-field THz communications in 6G and beyond. UE: User equipment; NLOS: non-line of sight; OAM: orbital angular momentum; MIMO: multiple-input, multiple-output; BS: base station.

We begin by explaining how signal propagation works in the next section. We introduce and explain the Huygens–Fresnel principle and explain why traditional array theory is no longer correct in the near field. We also highlight exactly the relations between the near and far fields and the commonalities that also exist, before explaining why THz communications must necessarily account for the near-field effect. In the section "Beamforming in the Near Field," we comprehensively explain what happens to canonical far-field beamforming that makes it ineffective in the near field. Specifically, we will show that the "pencil-thin beam" is instead a wide beam, and the gain is quickly saturated to a point at which the effectiveness of beamforming in improving the SNR does not work as expected. We provide experimental validation of these observations by analyzing the THz channel in the near field of large continuous-aperture horn lens antennas (11.8 cm in diameter) as well. In the section, "Near-Field THz Beams," we explain how the wavefront

can be manipulated to generate other beams. Specifically, we cover beamfocusing, Bessel beams, and Airy beams. We also explain the devices capable of generating these beams, along with their limitations, before delving into the bandwidth constraints of these beams. Notably, we also include a specific discussion on the design of the receiver, which hasn't been studied well in other tutorials. In the section "Applications in Common THz Issues," we expand upon recent progress and perspectives in how these beams can solve pressing issues in THz wireless, specifically 1) increased radiation gain or energy efficiency, 2) mitigation of blockages and improving NLOS links, 3) increased bandwidth utilization without sacrificing system capacity, and 4) increasing physical layer security through beamswitching. In the section "Research Challenges and Opportunities," we describe the latest pressing challenges and opportunities with near-field THz, and we finally end our manuscript with the section "Conclusions."

The tutorial is meant to present a look of "where we are now" rather than being another tutorial that champions one specific type of near-field wireless design. The present tutorial should boost further research in the novel area of EM information theory in combining electromagnetics and communications for physical layer design in 6G and beyond wireless systems.

Understanding signal propagation

Signal propagation

The models of wave propagation are founded upon Maxwell's equations. This simply means that as long as an EM wave can satisfy the paraxial wave equation, it is a valid way of propagating a signal [12]. The signal may be generated by a radiating aperture (such as a horn antenna, a lens, or a combination of the two) or by an array (which is a discretized summation of individual elements). In both cases, the fundamental aspect is based upon the linear superposition of EM waves, which states that, in the presence of a number of sources, the field at a given point in space is the complex vector sum of the fields from each of the individual sources [18]. Since a wave that propagates a distance of λ acquires a phase of 2π, the relative distance of the sources from this point in space as well as the initial phase at the sources themselves will both play a role in how the superposition occurs. While EM waves are complex vector quantities, for the discussion to be more simplified, we currently omit the aspect of polarization. Thus, the fields are treated as complex-valued scalars.

Array theory

Conventionally, we relied on array theory to provide us with the linear superposition principle. The fundamental postulates of array theory are that 1) the individual elements are radiating antennas, with the element size in the order of λ, where λ is the wavelength, and 2) array theory tries to present the resultant EM field in a specific direction, in spherical coordinates, assuming that we are extremely far away from the source of the radiation. The resultant beam that is generated by utilizing array theory is classically also known as *beamforming*, a fundamental axiom of nearly all modern wireless communications. For an array aperture that has M, N elements in the xy plane, the resultant array factor is given as [12]

$$A(\theta,\phi)=\sum_{m=1}^{M}\sum_{n=1}^{N}A_{mn}\exp(-jk[md_x\sin\theta\cos\phi + nd_y\sin\theta\sin\phi]) \quad (1)$$

where A_{mn} is the complex amplitude of the (m, n)th element. Notice that the field has spherical coordinates, where θ specifies the angle of orientation with the z-axis and ϕ the angle with the x-axis. When we apply the array factor with a specific radiating element, we can then multiply the array factor with the radiation pattern of the single element to gain the overall radiation of the array.

The Huygens–Fresnel principle

When the region of concern is closer to the radiating aperture, there is a more exact methodology for calculating the resultant EM field. This was provided by Christiaan Huygens in the form of the Huygens–Fresnel principle. The principle states that any given beam has a wavefront: an imaginary line that connects all of the points of the beam with the same phase. Now, every wavefront can be thought of as a secondary collection of infinitesimally small point sources, or wavelets, that radiate EM waves in a hemisphere in the forward direction. Thus, the beam is generated by following the coherent addition of the radiation from each of these wavelets. This methodology allows us to find the EM wave at any given location in space from a given distribution of the electric field at the source aperture. Here, EM scalar diffraction theory is utilized to evaluate the complex amplitude $A(x,y,z)$ of the EM wave with a wave vector k at any point from a given field distribution $A(\xi,\eta,0)$ generated across an aperture (ξ,η) orthogonal to the wave propagation direction z [13]:

$$A(x,y,z)=\frac{1}{j\lambda}\iint_S A(\xi,\eta,0)\frac{\exp(-jkr_1)(1+\cos\psi)}{2r_1}d\xi d\eta. \quad (2)$$

In simple terms, ξ and η are used as substitute variables for the x and y components of the aperture, respectively. Without loss of generality, the aperture is assumed to be orthogonal to the z-axis and located at $z = 0$, similar to the orientation specified when we discussed beamforming. The complex electric field distribution across the aperture is defined as $A(\xi,\eta,0)$, which is what will generate the EM wave. The complex amplitude of this electric field at all other positions, $A(x,y,z)$, can then be found by (2). In (2), $\cos\psi$ and r_1 both specify the information about the orientation and distance of the point (x, y, z) from the aperture spot (ξ,η). More specifically, r_1 refers to the distance from the points on the aperture $(\xi,\eta,0)$ to the point (x, y, z) where we are interested in evaluating the electric field. The angle ψ within $\cos\psi$ is the angle that the position vector of r_1 would make with the z-axis. Thus, the $1+\cos\psi$ term helps to capture the angular spread of the beam for points as we move further away from the z-axis. The complex field $A(\xi,\eta,0)$ is given as $\S\exp(j\Phi)$, where $\S$ is the magnitude and Φ is the phase across the radiating aperture. Thus, once we

have described the electric field, by knowing the phase variations across the electric field, we can keep track of the wavefront of the generated beam. It is noted that we assume the radiating aperture to be in the xy plane, and the signal propagates across the z-direction. We assume this setup, without loss of generality, throughout the rest of the manuscript.

It has been conclusively shown that, when the EM field from array theory is represented in Cartesian coordinates, and the field from the Huygens–Fresnel principle is simplified in the case of $r_1 >> x,y >> (\xi,\eta)$, the two produce the same result. Thus, we utilize the result from (2) as the guiding principle when building the case for signal propagation in this manuscript. This now allows us to present a common thread that ties all of the beams: their corresponding wavefront. Interestingly, although we assume continuous surfaces as we now utilize the Huygens–Fresnel principle, we note that this isn't necessarily required. In fact, the electric field distribution for the aperture in (2) can have spatially discrete radiating elements. All that would change is that the contributions of the empty spots as we move across the surface of the aperture in $\xi,\eta,0$ would be null, and thus the description of the electric field would be more complicated. We simply utilize continuous surfaces since we are more interested in the quantifying properties of the beams that we can create, and since these are still perfectly valid when we consider horn lens antennas and 3D-printed lenses, the discussions aren't impractical either.

Wavefronts as a part of the transmitted signal

We observe that while the Huygens–Fresnel principle specifically provides a manifestation of the wavefront within the complex phase profile of the input electric field, this kind of complexity has been absent from conventional communications. In fact, in nominal channel modeling, it was possible to completely decouple the antenna from the signal propagation, where we could consider the channel to have spherical wavefronts due to an omnidirectional antenna, and then focus specifically on the channel response. However, as we highlight in the section "Beamforming in the Near Field," it isn't trivial to design the THz channel agnostically of the antenna specifications. Thus, in our discussions, when we refer to the wavefront, we refer to the actual wavefront that is implemented at the antenna or the radiating surface aperture. This is convenient since this also allows us the most straightforward way to express how to generate other beams—we simply need to change the input electric field profile. The only modification that needs to be made in our approach is to now recognize that exotic wavefronts are possible, and when we discuss spherical wavefronts, these are actually being induced at the antenna through a specific type of electric field profile and not because of the channel.

Near field and far field

Array theory assumes the radiating aperture to be infinitesimally far away from the reference point at which the EM field is calculated, and it is specified in spherical coordinates. The Huygens–Fresnel principle provides us with a methodology to calculate the field exactly in Cartesian coordinates even within the finite distance around the radiating aperture. This turns out to give us a few regions of interest that are defined as the near field and the far field, with the near field further broken down into the reactive near field and the radiating near field. A quick summary is shown in Figure 2.

Near field

The near-field region has reactive and radiating components. The reactive region is extremely small and depends on the individual elements themselves, and it is a region where the waves are not yet decoupled from the antenna [13]. While used in power transfer, this isn't our subject of interest in this manuscript.

The radiating near field is the region of an array where the waves are decoupled from the antenna, but the size and field distribution at the array can significantly alter the type of beam generated in the near field. The wavefront can have many different shapes, leading to exotic beams, as discussed in detail in

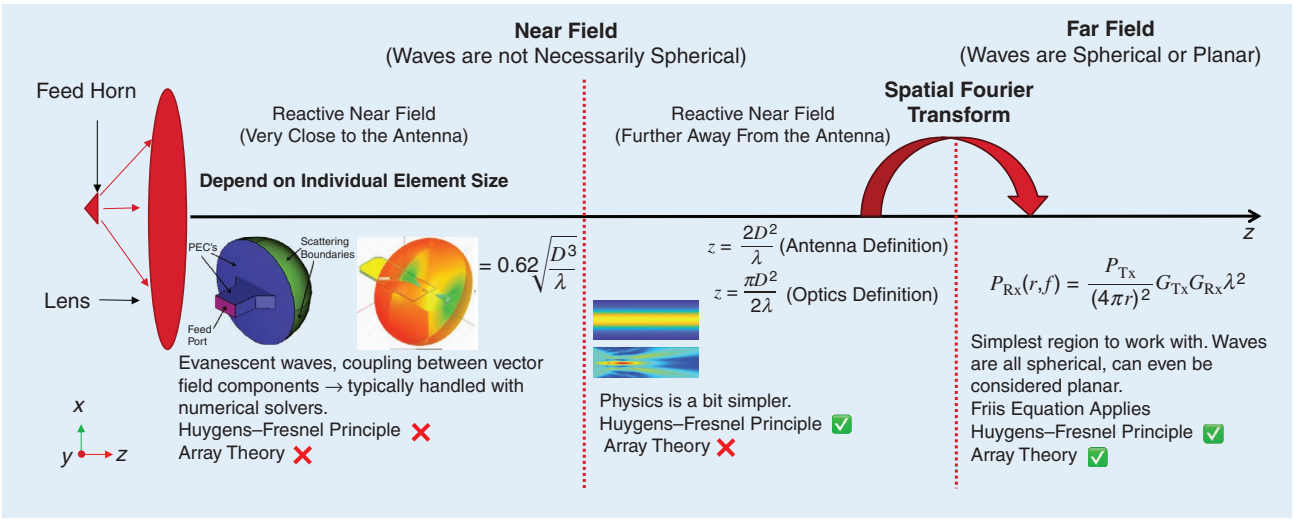

FIGURE 2. The reactive near-field, radiating near-field, and far-field regions of radiation from an aperture, such as a horn lens antenna, are considered. The aperture is situated in the xy plane, radiating in the z-axis. The radiating near field and far field are related via the spatial Fourier transform of the beam patterns. PEC: perfect electric conductor.

the section "Near-Field THz Beams." The simplifications from array theory yield considerable inaccuracies, as discussed in detail in the section "Beamforming in the Near Field."

Far field

The far-field radiation region is where the common terminologies of the Friis path loss as well as beamforming are well and truly applicable [12]. In communications, the radiating far field begins at a distance equivalent to the Rayleigh distance from an aperture. For a radiating aperture where D is the largest dimension, and λ is the signal wavelength, this distance is given by $2D^2/\lambda$. So, what is special about this distance? If we were to measure the path difference from the observation point at this Rayleigh distance to the closest and furthest points at the radiating aperture, the maximum distance would be limited to $\lambda/16$ (see the section "Gaussian Beams"). This means that the maximum path difference to the observation point is $\pi/8$ radian, which is sufficient to then assume parallel paths or the plane-wave assumption. A key point to note is that the far field and near field are interrelated via the spatial Fourier transform [12]. Thus, for example, if we desire an ultradirectional pencil-thin beam in the far field, we would require either an ultrabroad planar electric field excitation in the near field or an extremely large aperture!

In the far field of a practical, limited-size aperture, we ultimately observe that the wavefront diverges because of the diffraction properties of EM waves. Ultimately, the wavefront cannot be contained ad infinitum within a specific region, and we get an outward, divergent spread of the waves.

Why do THz systems have to be near field?

Let us understand exactly why THz systems need to be near field. Consider the communications system presented in Figure 3. The near field is understood as a region of communication where the transmitter and receiver are separated by a distance that ensures that if we were to measure the path difference from any point at the receiver to the closest and furthest points of the transmitter, the maximum difference in path length would be limited to $\lambda/16$. Thus, when we extend this definition to compare the near field between two radiating apertures and enforce the same conditions of maximum path distances being less than $\pi/8$ radian, the corresponding near field is significantly increased to

$$d_{\mathrm{F}} \approx \frac{2\left(D_1^{(r)} + D_2^{(r)}\right)^2}{\lambda} = \frac{4(D_1 + D_2)^2}{\lambda} \tag{3}$$

where d_{F} is the Rayleigh distance and D_l, D_2 are the dimensions of the arrays. We leave the reader to peruse the precise derivation in [19]. Thus, we now consider a THz system that must simultaneously fulfill the criterion of being in the far field when the communication distance is $d_{\min}$, while also simultaneously providing the required threshold SNR SNR_{SL} when the communication distance is $d_{\max}$. In this setup, we obtain a requirement on the size of the arrays D_1, D_2:

$$D_1 D_2 \geq \lambda d_{\max} \sqrt{\frac{N_{\mathrm{F}} k_B T B}{P_{\mathrm{Tx}}}}\, 10^{\frac{S_{\mathrm{L,dB}}}{20}} \tag{4}$$

where $N_0 = B N_{\mathrm{F}} k_B T$, with N_{F} as the noise factor, k_B the Boltzmann constant, and T the system temperature in Kelvins. B stands for the bandwidth of the transmitted signal in hertz, and P_{Tx} is the transmit power of the signal, while $S_{\mathrm{L,dB}}$ is the SNR threshold, S_{L}, in the decibel scale. Similarly, to satisfy the far field by the minimum distance $d_{\min}$ requirement, we have

$$d_{\min} \geq 4(D_1 + D_2)^2/\lambda \tag{5}$$

which we refer to as *Condition 1*. Hence, $(D_1 + D_2) \leq \sqrt{\lambda d_{\min}}/2$. Thus, a reliable mobile THz system as in Figure 3 must then satisfy both *Condition 1* and *Condition 2*:

$$\begin{cases} D_1 + D_2 & \leq \dfrac{\sqrt{\lambda d_{\min}}}{2} \\ D_1 D_2 & \geq \lambda d_{\max} \sqrt{\dfrac{N_{\mathrm{F}} k_B T B}{P_{\mathrm{Tx}}}}\, 10^{\frac{S_{\mathrm{L,dB}}}{20}}. \end{cases} \tag{6}$$

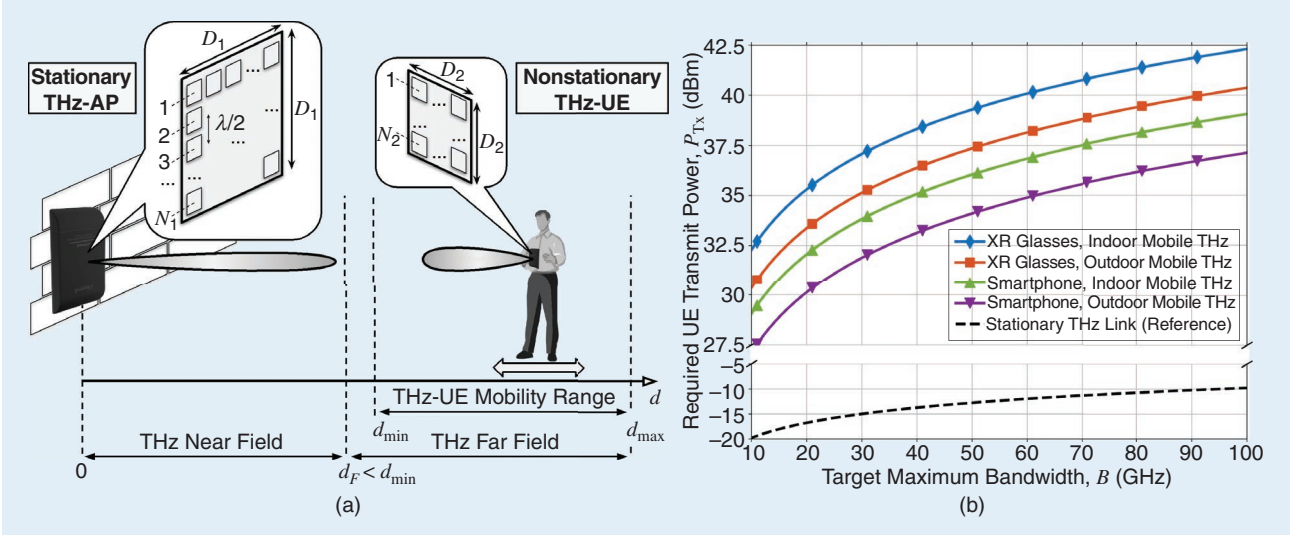

FIGURE 3. (a) Near-field versus far-field distance scenario for mobile user. (b) The power requirement to maintain the link in the far field is too exhaustive for wireless users. AP: access point.

When we solve these conditions simultaneously, we observe that the following restriction for the signal bandwidth, B, is formulated:

$$B \le (P_{\mathrm{Tx}} d_{\min}^2) \Big/ \left(256 d_{\max}^2 10^{\frac{S_{\mathrm{L,dB}}}{10}} N_{\mathrm{F}} k_B T\right) \tag{7}$$

which reaches the maximum when $D_1 = D_2$, or the access point and user equipment (UE) sizes are equal. However, such a condition is possible practically only when we think of stationary communications between base stations. When considering mobile THz links, where the base station is larger than the UE and the UE is also moving, the following two penalties are imposed on the possible bandwidth, leading to the following maximum bandwidth of a mobile THz system that satisfies both the SNR and the far-field requirements:

$$B_{\mathrm{Mobile}}^{(\max)} = B_{\mathrm{Stationary}}^{(\max)} \Big/ \left(M^2 \frac{(L+1)^4}{16L^2}\right). \tag{8}$$

Here, we have incorporated the *antenna inequality coefficient* $L = D_1/D_2$ and the *mobility coefficient* $M = d_{\max}/d_{\min}$. For practical sizes, we can see from Figure 3 that the power requirement is simply too massive to facilitate mobile THz links without reducing the requirement that THz links be exclusively far field. Thus, THz wireless must be near field! Therefore, near field plays a crucial role in maintaining link reliability for sub-THz, THz, and, hence, next-generation wireless systems.

Beamforming in the near field

Here, we investigate the practical limits of near-field beamforming.[1] First, we recall the Huygens–Fresnel principle from the section "Understanding Signal Propagation," which allowed us to bring forth the idea of a wavefront. This then allows us to represent the transmitter through an electric field distribution that is creating the specific EM wave.

The Huygens–Fresnel principle shows that the characteristics of a beam generated by a radiating aperture are completely defined by the phase and amplitude distribution of the electric field at the radiating aperture [13]. This is understood by assuming that each point on a radiating aperture emits the signal like a point source or a wavelet. Then, the beam is defined by the superposition of all of the individual wavelets, creating the direction of propagation of the beam. Therefore, to generate any of the beams, all that is required is the corresponding wavefront, which can be engineered by a specific phase profile. In addition to implementing this through an array, the same is also possible through custom-designed lenses or in reflection through the utilization of reflectarrays and metasurfaces. We discuss this in more detail after introducing the different beam types. For all discussions, without loss of generality, we assume the beam to be generated outward in the z-axis. The array is assumed to be in the xy plane. Thus, the electric field across the aperture is defined with the x and y Cartesian coordinates, generating a beam in the z-axis. Note here that we only consider broadside beamforming and not beamsteering in directions away from the broadside. When we highlight the shortcomings of beamforming in the near field, we are keeping the discussion to the most general case, which highlights why the beam is inefficient before we add the increased complexity of nonbroadside mobility. We expand more on this challenge in the section "Research Challenges and Opportunities."

Beamforming

We consider far-field beamforming and observe what happens to this phenomenon within the near field. We know that beamforming is a straightforward superposition of EM waves, generated when the entire radiating aperture is excited as a plane wave or with a uniform phase. Since we consider an aperture in the xy plane, we can define the electric field that is set up across this aperture that will give rise to the EM wave. The arbitrary electric field $E(x, y)$ is given as

$$E(x,y) = E_0 \exp(jk(\phi)) \tag{9}$$

where E_0 is the initial electric field, and ϕ is the phase variation, with k specifying the wave vector. Generally speaking, ϕ would be some function of x, y, thus creating a nonuniform electric field across the aperture. However, in the case of beamforming, we require a uniform phase with $\phi = 0$, and the resultant electric field distribution is given as $E(x,y) = E_0 \exp(jk(\phi)) = E_0$ (there is no variation in the phase across the electric field aperture).

Going from the far field to the near field

In the far field, the beam's response is determined by a sinc function, as specified by the array factor. Here, the width of the first maximum of the sinc function defines the beamwidth, with the other zeros all defining corresponding sidelobes [12].

The question now is: What would the near-field response look like? Here, we remember that the near field and far field are interrelated via the spatial Fourier transform. That is, if we obtain the expression of the far-field signal and apply the Fourier transform, we obtain the near-field representation. This is analogous to the temporal Fourier transform. However, we now go from the space domain to the wavenumber domain. Thus, a far-field sinc function (signal in space) is generated by a rectangular input electric field (wavenumber domain), as shown in Figure 4. Mathematically, we can show that $2.w_0.\mathrm{sinc}(Sw_0) \Leftrightarrow \mathrm{rect}(s/2w_0)$, where $2W_0$ is the antenna aperture and S and s are spatial wavenumber and wavenumber variables for near-field and far-field waves, respectively. In particular, the near and far fields are mathematically interconnected through the spatial Fourier transform, allowing one to demonstrate the properties of the other. The larger the rectangular aperture electric field, the wider the rectangular input size, and the narrower the width of the far-field sinc function (increased directivity) [12], [20]. Indeed, this is exactly what happens when we utilize a larger aperture. As shown in Figure 4, the initial beam is exactly the size of the radiating

[1]Several investigations in the literature interchangeably utilize near-field beamforming with spherical-wave beamfocusing (described in the section "Beamforming in the Near Field") as well. However, when we refer to near-field beamforming, we refer to beamforming in the near field, i.e., that which happens when canonical beamforming is attempted in the near field.

aperture, with the far-field representation defined per the sinc function. So, how do we study the near-field equivalent? It turns out that if we consider a radiating aperture of size $D = 2w_0$, the near-field equivalent is the corresponding Gaussian beam with a beam waist of w_0.

Gaussian beams

A Gaussian beam, as shown in Figure 4, is the near-field equivalent of beamforming. When generated from an aperture of size $2w_0$ situated within the xy plane, with an initial electric field E_0, the field $E(z)$ after propagation in the z-axis is given as

$$E(z) = E_0 \frac{w_0}{w(z)} \exp\left(\frac{-r^2}{w(z)^2}\right) \exp\left(-j\left(kz + k\frac{r^2}{2R(z)} + \phi(z)\right)\right)$$
$$\text{where } w(z) = w_0\sqrt{1+\left(\frac{z}{z_R}\right)^2},\ R(z) = \frac{z^2+z_R^2}{z}. \tag{10}$$

In (10), w_0 is the beam waist, and $R(z)$ is the radius of curvature, with $\phi(z) = \arctan z/z_R$ describing the Gouy phase. The beam waist is defined as the region of the beam where the beam is most tightly focused, with the radius of curvature being infinite. Once the beam begins to propagate in the z-direction, we note that the beam spreads in the region of $w(z)$, and the radius of curvature changes as well. The Gouy phase is a parameter that is most useful immediately near the generation of the beam ($z \approx 0$), and it helps to explain some of the effects that a Gaussian beam undergoes in extremely precise optical experiments. For all practical intents in our discussions, the Gouy phase can be assumed to almost always be a constant. The variable r is the radial cross-sectional distance from the z-axis, satisfying the Cartesian relation $r^2 = x^2 + y^2$. When this beam is incident upon a receiver, the received power P_{Rx} is then simply the integral of the radiated intensity of the EM wave with wave vector k_0 over the receiver aperture S_{Rx} with free-space impedance Z_0:

$$P_{\text{Rx}} = \frac{1}{2Z_0}\iint_{S_{\text{Rx}}} |E(z)|^2 dS_{\text{Rx}} \tag{11}$$

where $E(z)$ is the electric field from (10).

It can be shown that approximately 96% of the power of the Gaussian beam is contained within $w(z)$. The Rayleigh range is given as

$$z_R = \pi w_0^2/\lambda \tag{12}$$

and describes the distance at which the beam waist w_0 spreads by a factor of $\sqrt{2}$. i.e., $w(z = z_R) = \sqrt{2}\,w_0$. At $z = z_R$, if we consider the same region of w_0, the power has roughly halved compared to the power within w_0 at $z = 0$ since the intensity has become proportionally weaker. The Rayleigh range, then, is a measure of how concentrated, or directed, the signal is. We see that the Rayleigh range depends on two key factors: 1) the original beam waist and 2) the wavelength. More specifically, the larger the beam waist at the point of generation, the slower the beam spreads. This is analogous to saying that larger aperture antennas (which will generate a beam with a bigger beam waist) give us more directivity (slower spread). At the same time, for a same-sized beam waist, the smaller the signal wavelength, the longer the Rayleigh range. This is also analogous since the same physical-size aperture has a higher gain (more directivity) for greater frequencies.

Observing the phase component of the Gaussian beam in (10), we can observe a factor of $k(r^2/2R(z))$, where k is the wavenumber, which varies across the cross-sectional aperture depending on r (remember that r here refers to the radial cross-sectional distance from the z-axis, satisfying the Cartesian relation $r^2 = x^2 + y^2$). Here, the term $R(z)$ refers to the radius of curvature. The radius of curvature is initially infinite, implying a planar wavefront immediately when the beam is generated (region B in Figure 4). Then, the radius of curvature reaches a minimum at the Rayleigh distance of z_R (region C in Figure 4) and finally begins to expand again as we enter the far field (region D in Figure 4).[2] In direct contrast to the radius of curvature, the wavefront either acquires a planar wavefront or a

[2]It is prudent to reiterate that the Rayleigh range is different from the near-field Fraunhofer distance. While the two have similar values and depend on similar factors (the size of the aperture and the wavelength), the two come from different aspects related to optics and communications, respectively. The Rayleigh range is the region where the beam waist has spread by a factor of $\sqrt{2}$. The Fraunhofer distance is, as mentioned in the section "Understanding Signal Propagation," the distance at which we can assume planar wavefronts with at most a $\pi/8$ error in phase discrepancy.

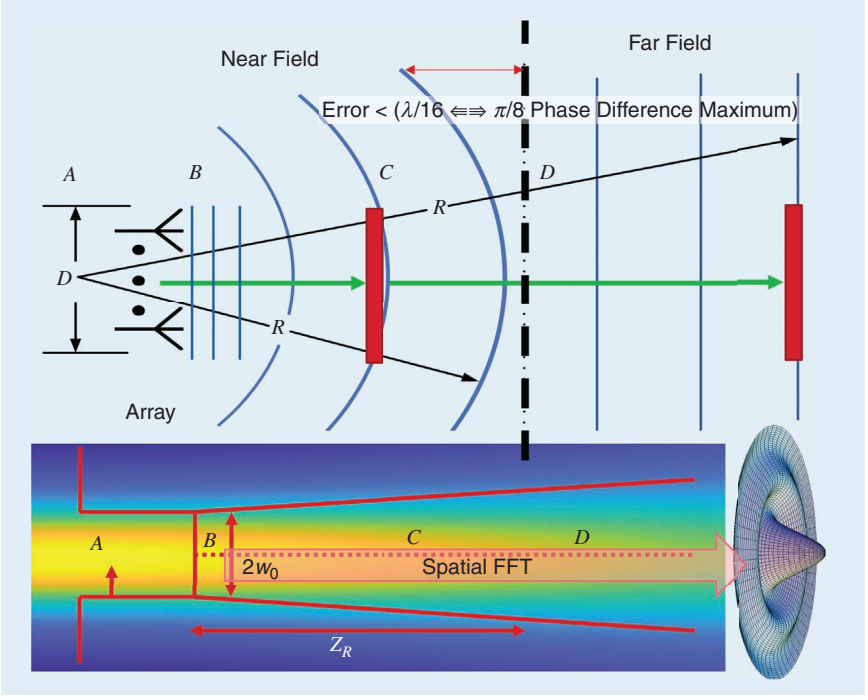

FIGURE 4. Equivalence of beamforming with Gaussian beams. FFT: fast Fourier transform.

more spherical wavefront. When spherical, however, the waves are concave, or spread outward.

When in the near field with beamforming, we see that the issue is that the minimum radiation coverage, or the beam waist, can be minimum to only w_0, which is the size of the radiating aperture. This is contradictory to the common assumption that with increasing size of the array, the gain of the transmitter reduces the beam waist infinitesimally [that is true only in the far field since then we are indeed reducing the spread as per (12)]. This is the fundamental limitation of canonical beamforming in the near field. An example of this is shown in Figure 5, with a 15-dBi antenna and a 38-dBi antenna being simulated and the corresponding beams shown. It is seen that, initially, the beam of the 15-dBi antenna is more concentrated than that of the 38-dBi antenna, but it spreads much faster. Conversely, the larger beam of the 38-dBi antenna distributes the power initially in a larger area, but the spreading losses are considerably reduced. The canonical understanding of the gain would state that the beam would be ultradirectional; however, that is only relevant in the far field, when we consider the directivity. In the near field, the beam has a larger beam waist, which spreads slowly. It is then obvious that, for a smaller receiver, only a small fraction of the beam is actually intercepted, drastically reducing the efficiency of beamforming. In addition, we can observe from the cross-sectional phase that a Gaussian beam does not have a uniform cross-sectional phase as it propagates. Thus, a larger receiver can intercept several out-of-phase components, again reducing the efficiency of the final power received. Without these critical understandings of the nature of the near field with beamforming, we could reach an erroneous conclusion that, quite unexplainably, the THz channel is more hostile to larger antennas [11].

THz channel with near-field beamforming

When beamforming, or when Gaussian beams are utilized, the larger aperture has a saturation gain that reduces the actual perceived gain of the antenna. At the same time, a larger receiver also captures more out-of-phase components of the radiated signal that is incident on it. This also effectively reduces the directivity of the antenna. Additionally, a larger beam waist can be reflected more effectively in the near field, increasing the likelihood of multipath effects, thus changing the *K*-factor as well as the delay spread. Analyzing these effects on the THz channel requires in-depth channel sounding, as demonstrated in [11]. We observe that the THz channel cannot be designed agnostically of the specifications of the antenna. Indeed, as evidenced through channel sounding measurements at 140 GHz, the key metrics of the antenna, including the path loss exponent (PLE), *K*-factor, and delay spread, all are dependent on the transmitter and receiver antenna. The path loss models are crucial to estimate power loss over the wireless interface due to multipath interference. The presence of an LOS component typically leads to the representation of path loss using the log-distance model. In this context, the path loss, PL, at a given distance d is determined by assessing it in relation to the Friis free space path loss, PL_0, at a reference distance $(d_0 = 1\ m)$. The additional loss incurred due to the distance, d, is characterized by a PLE, denoted by the symbol n. Furthermore, to account for the shadow effect, a zero-mean Gaussian distributed random variable, χ, characterized by a standard deviation of σ dB, is introduced. The cumulative PL is expressed as a function of these factors and given by

$$\mathrm{PL} = \mathrm{PL}_0 + 10n\log_{10}\left(\frac{d}{d_0}\right) + \chi. \tag{13}$$

The value of n was determined through the correlation of the experimental path loss, denoted as L_{PL} on the dB scale, with the model specified in (13). It was observed that, with more directive antennas, the calculated path loss escalates, exhibiting a higher PLE, as depicted in Figure 5. This observation suggests a greater channel loss, attributable to near-field effects that diminish beamforming efficacy and, consequently, antenna gain. Clarity emerges upon scrutinizing the spreading

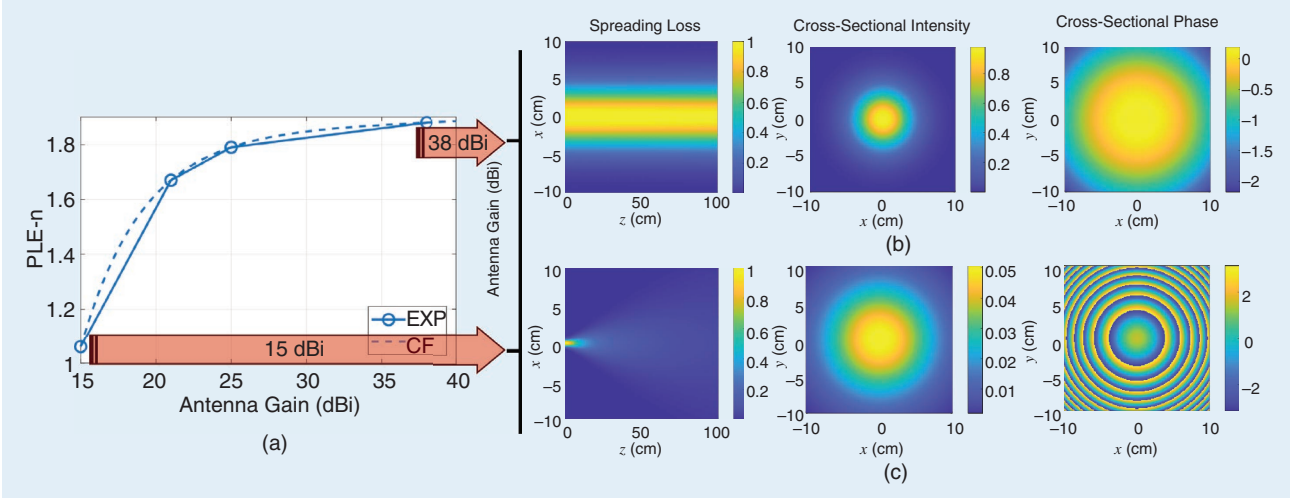

FIGURE 5. (a) Experimental and curve-fitted PLE with varying antenna gains for indoor setups. The beam profile of (b) 40-mm and (c) 4-mm aperture antennas with propagation, cross-sectional amplitude, and cross-sectional phase at 300 GHz (cross-sectional cut at 1 m). PLE: path loss exponent; EXP: experimental; CF: curve fitted.

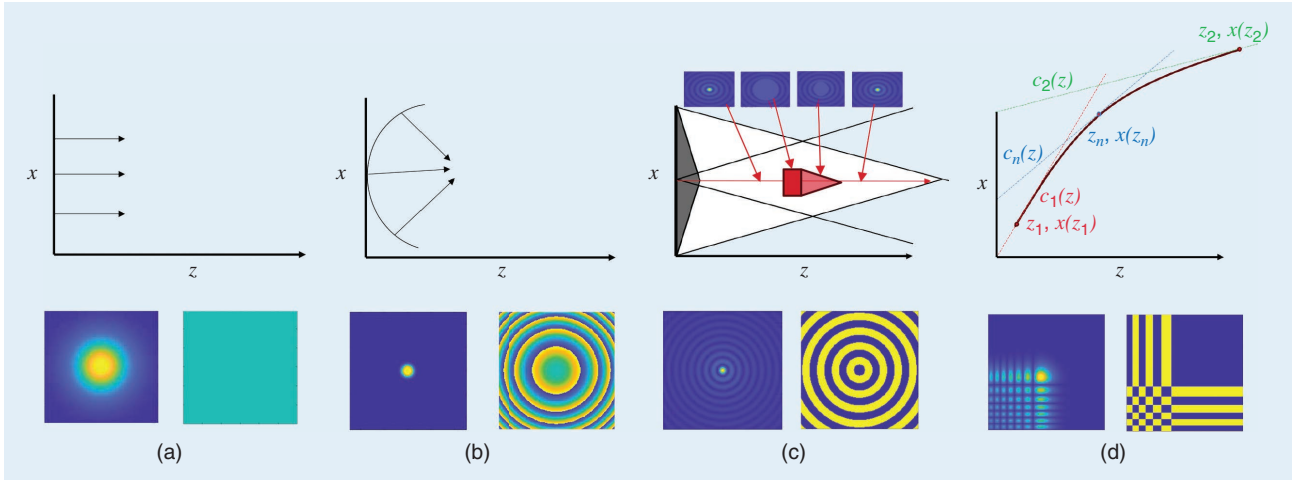

FIGURE 6. Wavefront engineering for creating wireless THz links, in which the beam profiles can significantly deviate from the Gaussian. (a) Beamforming, (b) Beamfocusing, (c) Bessel beam, and (d) Airy beam. The cross-sectional intensity and phase of each beam are also shown. The aperture is in the xy plane, radiating in the z-axis.

loss, incident intensity, and phase across varied antennas, as depicted in Figure 5 for 15-dBi and 38-dBi antennas, furnishing a more perceptible comprehension. The 15-dBi antenna shows the effects that we would expect from canonical beamforming, even within indoor setups, as the near-field region is very small. However, with the 38-dBi antenna, it is seen that the near-field region extends well into several meters, and thus the corresponding propagation, cross-sectional intensity, and phase profile are not as expected. Ultimately, even though we are free to utilize beamforming in the near field, we are not free from the consequences: drastically wider beams that hinder the receiver SNR, thereby reducing the possible utilizable bandwidth while also potentially increasing security concerns.

Near-field THz beams

We understand that an exclusively far-field THz system cannot afford mobility or practical sizes for the user interface. Further, in the near field, beamforming reaches saturation gain, and the THz channel cannot be evaluated without an understanding of the antenna effects. Thus, we now introduce and explain different wavefronts that can realize robust THz communications. The discussed THz wavefronts are illustrated in Figure 6, and their key features are summarized in Table 1. We consider the radiating aperture to be in the xy plane, and consider the beam propagating in the z-axis. When discussing the beams, we consider continuous apertures, such as horn lens antennas with custom 3D-printed lenses, which have already been demonstrated in several experiments to generate these beams. The continuous aperture allows us to focus on the specific properties of the beams, rather than the design methodology of the array and how this could impact the beam. Nonetheless, we do discuss different strategies in generating the beams in the section "Wavefront Generation."

Beamfocusing

Given a transceiver system, the most intuitive method of signal propagation would be to focus all of the energy toward the transmitter. This methodology is called *beamfocusing*. In beamfocusing, the objective is to focus the energy from the transmitting aperture toward the receiver. The analogy is equivalent to mimicking a lens, with the receiver at the focal point. For this, the electric field across the transmitter should have a spherical wavefront, given as $E(x,y) = E_0 \exp(jk(\sqrt{F^2 + (r^2)} - F))$, where $r = \sqrt{(x^2 + y^2)}$ is the radial distance and F is the focal point. k refers to the wave vector given as $2\pi/\lambda$, where λ is the signal wavelength. This is thus a convergent spherical wavefront, which will reach a singularity at F.

Beamfocusing can thus be understood to be like a spotlight that is directed toward the receiver [8]. It has been extensively studied in the literature recently, as the prevalence of near field in THz communications has become understood. In [9], it is shown that beamfocusing provides not just angular but also distance-dependent resolution, which can lead to opportunities in multiplexing multiple receivers. At the same time, [8] also discussed novel opportunities for avoiding eavesdroppers through near-field security; this is possible because of the focusing nature of the radiation. This can also increase the energy efficiency of the system. However, beamfocusing has little resistance to micro or macro mobility since the nature of focusing requires that the channel state information be constantly updated to ensure that the receiver is within the "spotlight" [9].

Table 1. Comparison of different near-field THz beams.

Type	Required phase	Beam profile		Blockage resilient	OAM	Energy efficient	Ultrabroadband
		Near field	Far field				
Beamforming	Planar	Gaussian	Sinc	✗	✓	✗	✓
Beamfocusing	Quadratic	Point	Undefined	✗	✗	✓	✗
Bessel beams	Conical	Bessel	Annular	✓	✓	✓	✓
Airy beams	Exponential	Airy	Undefined	✓	✓	✓	✗

The size of the spotlight is given via the Abbe limit, which is expressed as

$$d = \lambda \frac{F}{D} \tag{14}$$

where d is the resolution spot, and F is the distance of the desired beamfocusing spot from the radiating aperture with a size D and design wavelength λ. Clearly, the further the focusing spot, the greater the spread of the beam spot. Interestingly, if we input the focusing spot as $F = \infty$, we see that the beam spot now becomes a general direction and becomes equivalent to beamforming. Indeed, this can also be understood from the spherical phase $\phi = \sqrt{F^2 + (r^2)} - F)$. If $F = \infty$, then we get beamforming. Note that the spherical wavefront is convex, or converging, and not diverging like that in near-field beamforming. This happens because beamfocusing must be engineered, while the divergence of beamforming is due to spreading losses.

If the focusing spot can be completely centered on the receiver, the energy efficiency can be increased, as evidenced in [8]. However, it also becomes important to understand that beamfocusing involves convex wavefronts incident on the receiver. Thus, the receiver needs to be designed such that it is coupled to the nonuniform wavefront. Ultimately, beamfocusing has promise in stationary, nonmobile situations where the transmitter and receiver can be preconfigured, but it does not appear to be the most practical choice when it comes to more ubiquitous THz wireless systems.

Bessel beams

Bessel beams are a subset of beams with the electric field given in cylindrical coordinates as

$$E_n(r, \phi, z) = E_0 \exp(-jk_z z) J_n(k_r r) \exp(\pm jn\phi) \tag{15}$$

where $J_n(.)$ is the nth-order Bessel function of the first kind [21]. Bessel functions are a class of functions that are a solution to the Bessel differential equation [4]. While convenient to express in cylindrical coordinates, we can easily transfer the beam profile in Cartesian coordinates by remembering that $r^2 = x^2 + y^2$ is the radial distance, and $\phi = \arctan(y/x)$ is the azimuthal angle. The cylindrical coordinate system allows us to utilize the radial symmetry of these beams more conveniently. As we will expand here, Bessel beams appear to be candidate beams for near-field THz solutions. These beams contain ring-shaped intensity and nonuniform phase profiles with radial step-like variation. The simplest solution of this beam equation is given by setting $n = 0$, giving the zeroth-order Bessel function [4]. This zeroth-order beam is generated via a radially symmetric linear phase profile, resulting in a conical wavefront. The conical wave vector k can be decomposed into the radial and transverse wave vectors k_r and k_z, respectively. The two are interrelated by $k^2 = k_r^2 + k_z^2$. As shown in [4], it is feasible to generate a Bessel beam with any radial wave vector $k_r < k$, at which point the wave does not propagate and becomes evanescent. Thus, in setting up a Bessel beam, the radial wave vector determines the intensity cross section through manifesting within the Bessel function, while the transverse wave vector manifests in the distance that the beam propagates.

As illustrated in Figure 6, the zeroth-order Bessel beam profile has a central bright spot along the cone axis, with multiple concentric rings around it, which are interference patterns created from the interference of plane waves from the opposite sides of this central axis. A Bessel beam is an exact solution to Maxwell's equations, where the beam has a constant intensity since it satisfies the wave equation. As the beam propagates, the cross-sectional intensity does not change and has no spreading loss. However, since the Bessel function is nonending, a true Bessel beam requires an infinite aperture with unlimited power [4]. Nonetheless, quasi-Bessel beams can be set up within the near field of a radiating aperture. For an aperture in the xy plane, the electric field $E(x,y)$ is set up to mimic plane waves traveling inward on a cone:

$$E(x, y) = E_0 \exp(-jk\sqrt{x^2 + y^2} \sin(\theta)) \tag{16}$$

where θ describes the angle of the realized cone and E_0 the magnitude of the field. Notice how we get a radially symmetric electric field since, once the cone angle θ is defined, the only variable is $r = \sqrt{x^2 + y^2}$. The beam dissolves into a diverging ring beyond a maximum distance of propagation $Z_{\max}$. For a finite aperture of size $2w_0$, this maximum distance of propagation is given as [2]

$$Z_{\max} = \frac{w_0}{\tan(\theta)} \tag{17}$$

where θ is again the cone angle. From the geometric relations explained in [7], we can also approximately model $Z_{\max}$ as [2]

$$Z_{\max} \approx w_0 \frac{k_z}{k_r} = w_0 \sqrt{(k/k_r)^2 - 1}\,. \tag{18}$$

Bessel beams propagate in the near field, a feature absent in beamfocusing, which does not propagate but converges at a focal point. In addition, as Bessel beams can be understood to be the interference pattern of plane waves traveling inward on a cone, they are resilient to blockage. Even if some of the waves are blocked by an obstruction, the remaining waves still reconstruct the interference pattern and help regenerate the Bessel beam after the obstruction; hence, they are also referred to as *self-healing beams* [22].

These features lead to an interesting design choice. The size of the central bright spot is directly provided by the solution of the zeros of the Bessel function. Since the Bessel function has the first zero at $J(x) = 0$ with $x = 2.405$, the size of the central spot is given as $a = 2.405/k_r$. From the relations outlined in [2], we can observe that, on the one hand, a larger central spot gives rise to fewer concentric rings but also helps the Bessel beam to propagate further. On the other hand, a larger number of rings theoretically leads to better self-healing capabilities.

Bessel beams can be utilized to create a higher depth of focus since the central lobe can be much more concentrated in power than the limit of beamforming. For this reason, Bessel beams can provide a higher SNR in near-field links even if

blockage is not a primary issue. This has been verified experimentally in [7], where it is shown that a 9-dB improvement is found when utilizing a Bessel beam in sub-THz links compared to a Gaussian beam. Bessel beams have previously been utilized in the optical regime and are not also being explored at millimeter-wave (mmWave) and (sub-)THz frequencies. All of these properties as well as a far simpler linearly varying phase profile (as opposed to the spherical requirement in beamfocusing) make Bessel beams a promising wavefront candidate for THz communications.

Curved and Airy beams

While Bessel beams can go "through" an obstacle, another class of beams can completely circumvent blockage while also potentially enabling NLOS links. These beams follow a curved trajectory, and when viewed from the transverse direction, the beams appear to have acceleration without any external energy—earning their classification as *self-accelerating beams*. Such beams have been recently demonstrated [5], where the beam profile is described with the Airy function. The Airy function is a solution to the Stokes equation [5]. The cross-sectional intensity of such Airy beams is illustrated in Figure 6(d), and these beams satisfy a solution to Maxwell's equations with an exponential cubic phase front. The electric field in one dimension is given as

$$E(x,z) = Ai\left(\gamma x - \frac{\gamma^4 z^2}{4k^2} + j\frac{\alpha\gamma z}{k}\right)\exp\left(j\Phi(x,z) + \alpha\left[x - \frac{\gamma^3 z^2}{2k^2}\right]\right) \tag{19}$$

where $Ai(.)$ is the Airy function [5]. The phase is given by $\Phi(x,z)$. The parameter α specifies an attenuation constant to make the energy requirement of the beam possible. The beam follows a curved path $x(z) = \gamma^3 z^2/4k^2$, with the initial electric field at $x,z = 0$ satisfying the amplitude $Ai(\gamma x)$ and phase $\arg(Ai(\gamma x))$. The curvature function depends on x_0, which is the initial placement of the beam on the aperture. The trajectory can be adapted based on the properties of the environment (e.g., the blocker location and size) for resilient, high-speed connectivity in sub-THz regimes [10], [14].

The required phase and corresponding wavefront to generate these beams can be found by first describing the desired curvature trajectory. Then, the principle of caustics from ray optics can be utilized to find the required phase. That is, we may first consider an arbitrary curve (see Figure 6). Then, tangents from the curve can be drawn to the aperture, and the required phase at that point in the radiating aperture is found as $\Phi(x)$ [14]

$$\Phi(x) = k\frac{d(x(z)/z)}{\sqrt{1 + dx(z)^2/z}} \tag{20}$$

where $x(z)$ defines the parabolic desired trajectory that we wish to engineer across the beam propagation. Although shown for a 1D aperture in the x-plane, it also easily extends to an aperture in the xy plane as well, as shown in [5] (see Figure 6). The important factor is that the greater the curvature, the larger the aperture size needed to fulfill the tangential requirements. As is obvious, an increased beam curvature requires both a steeper phase progression across the array aperture as well as a much larger aperture size. These beams are extremely promising to avoid blockage, and can also be utilized to curve around corners, enabling potential NLOS links. Since the angle of arrival can be changed when incident upon the receiver, these beams can also be utilized for beam alignment and link monitoring.

Wavefront generation

Once the appropriate beam type is selected, the corresponding wavefront can be identified by following the Huygens–Fresnel principle. However, on the one hand, beamforming antenna arrays at THz frequencies are still under development, and on the other hand, phases are discretized both spatially because of both the size of the antenna element and also the sampling limitations of the corresponding phase shifter [13]. In this context, graphene-based plasmonic antenna arrays have also been proposed [1]. It has been shown that these antennas can be up to an order of magnitude smaller than a conventional patch antenna, allowing for dense integration within an array. With the plasmonic modulator, it becomes possible to apply any phase across the radiating element, thus providing adequate support for the nonlinear phase requirements of beamfocusing and Airy beams, in addition to the linear ramp of Bessel and beamforming.

Taking this concept further still, metasurfaces can also be utilized to generate near-field beams [1], [23]. These are tightly coupled 2D counterparts of metamaterials, where a sub-wavelength radiating element—usually a metal half-ring—is utilized to produce a particular radiation pattern. With metasurfaces, the radiating element can reach the level of a wavelet—being extremely small. However, the drawback is that the entire metasurface response is configured at once, and thus it isn't straightforward to find the phases and required configuration of applying the wavefront required to generate a particular beam. Further yet, metasurface designs are heavily frequency dependent; thus, just because a design works at one frequency doesn't mean it can be scaled to another. Instead, significant reworking is required whenever the design parameters, such as the signal wavelength or bandwidth, are changed. Nonetheless, metasurfaces have great potential for use in near-field radiation, and their design is a subject of active research.

In addition to active arrays and metasurfaces can also be utilized in reflection, whereby a reconfigurable intelligent surface (RIS) can be utilized to impart the necessary phase on a beam that is incident upon it [1], [7]. At the same time, it becomes possible to design and 3D-print a specific lens that can be fitted atop a large horn lens antenna or to utilize a complicated antenna configuration, such as a radiating dish [7], [13]. Here, the resolution of the lens plays a role in how well the beam is generated. Notably, this is how the majority of experimental works are being validated since the design process is much simpler and can be completed with currently available technology. For example, the work in [7] utilized a 3D-printed lens mounted atop an 11.8-cm-wide horn lens antenna to generate an ultrabroadband Bessel beam (20-GHz bandwidth and

140-GHz carrier) and validate some of the specific properties discussed previously.

Wideband limitations

Wavefront engineering is, at its core, a narrowband concept. As the reader might observe, we have described all of the preceding beams with a clear wave vector response, defined at k_0. Thus, when a signal with a bandwidth of $f_{\min}, f_{\max}$ is utilized, it naturally leads to a question as to how much bandwidth can be supported for the different wavefronts. Per the Huygens–Fresnel principle, each wavelet (or element) of a radiating aperture emits an EM signal. The superposition of these signals from all of the wavelets then describes the amplitude of the EM signal as generated by the total aperture. The resultant radiation can be manipulated through the application of a set of time delays across the wavelets to have coherent addition at the receiver. The time delay δt is often approximated through a phase delay $\delta\phi = kc\delta t$, where k is the wave vector and c is the speed of EM waves.

Thus, once the phases are decided upon per the desired beam, they are applied across the electric field of the radiating aperture. We can simply focus on the phase variations by specifying a codebook for the aperture that captures the phase variations across the aperture. This phase codebook $C(\Phi)$ is a function of the spatial arrangement of the aperture, which involves phase delays across the aperture that are a function of the wave vector: $C(\Phi) = f(x, y, k)$, where k is the wave vector and x and y refer to the arrangement of the aperture. Now, we focus on the variation in the wave vector as we consider the bandwidth of the system. In a wideband system, the bandwidth of the system is $B = [f_{\min}, f_{\max}]$, centered around a design frequency f_0. Thus, the codebook is designed as per the central wave vector k_0, or $C(\Phi) = f(k_0)$, that is then unchanged across the range of the frequencies. The equivalent codebooks $C(\Phi)_k$ that are then effectively applied to the other frequencies of this wideband system depend on both this "central codebook" $C(\Phi)$ as well as the deviation of the wave vector from this design wave vector:

$$C(\Phi)_k = f(\alpha, C(\Phi)) \tag{21}$$

where $\alpha = k/k_0$ is the ratio of how far from the design frequency we are investigating the codebook.

Effect on beamforming and beamfocusing

When beamforming is broadside, there is no phase being applied at the wavelets, and thus there is no wideband limitation—a special case. However, it is relevant to note that the inefficiency of beamforming is still a pressing issue. When the beam is steered away from the broadside, there is a linear phase applied across the beam, which leads to the beamsquint effect. Beamsquint has been studied in the past as it is a well-understood phenomenon in far-field beamforming [12].

In beamfocusing, the signal is focused at a particular spot. Thus, when a larger bandwidth is utilized, we now observe a beamsplit effect. Here, frequencies with wave vectors of k are now focused at different points [8]. The focusing spots are deviated from the desired focal spot by a distance that is proportional to the ratio k/k_0, where k_0 is the design wave vector. This thus serves to reduce the efficiency of wideband beamfocusing. At the same time, however, this technique has been proposed for near-field MIMO where several receivers in the same coaxial plane can be serviced simultaneously by different subcarriers of a multicarrier signal, owing to the fact that the beamsplit effect will naturally separate the carriers [8]. However, when a high bandwidth is required, this becomes a pressing issue.

Effect on Bessel and Airy beams

Bessel beams are analogous to plane waves traveling inward on a cone, where the cone angle is defined per the ratio of the radial wave vector k_r to the transverse wave vector k_z, satisfying $\sqrt{(k_r^2 + k_z^2)} = k^2$, where k is the wave vector. Thus, in the case of Bessel beams, the wideband effect changes the effective angle of the cone, thereby altering the propagation range of the Bessel at that particular frequency. Nonetheless, for every frequency, it is guaranteed that there will be constructive interference along the direction of the Bessel beam (analogous to plane-wave beamforming) [7]. More importantly, we observe that, as the cone angle becomes reduced, we get a longer propagation, and as the cone angle sharpens, we get a reduced propagation distance. Interestingly, it so happens that the frequencies that are above the design frequency (with the corresponding wave vector $k < k_0$) propagate further than the frequencies below the design frequency. Thus, if considering a system with a bandwidth of $B = [f_{\min}, f_{\max}]$, it may be suitable to characterize the propagation distance for $f_{\min}$ since that will automatically ensure that all of the other frequency components will reach the receiver.

In the case of Airy beams, we observe that the phases represent the tangents to the curve that we would like the Airy beam to propagate across. Thus, when the effective phases change, the tangential points change. This leads to a near-field dispersion effect, similar to the rainbow spectrum observed in leaky wave antennas (albeit at much less pronounced bandwidths) [12]. Therefore, in the near field, the instantaneous bandwidth is defined as [14]

$$\Delta f = \frac{zf_0}{\sqrt{z^2 - 2k_0^2 x_0^3 D}} - \frac{zf_0}{\sqrt{z^2 + 2k_0^2 x_0^3 D}} \tag{22}$$

where $D = 1.63x_0$ is the full width at half maximum of the main lobe, f_0 is the center frequency, and k_0 is the central wave vector, with x_0 specifying the curvature parameter.

Orbital angular momentum: Exploiting new properties

The properties of wavefronts present opportunities for the development of new communication methodologies. Among the distinctive properties found in specific EM waves is the manifestation of orbital angular momentum (OAM), initially demonstrated in [3]. OAM-carrying beams exhibit a spiral phase in the transverse direction, featuring a helical wavefront. Consequently, the central axis of this helix consistently maintains zero intensity, leading to the designation of these beams as vortex beams. It is important to clarify that, while the OAM exists as a property of the wave, it is not a wavefront itself. Rather, the wavefront exhibits a helical structure with a spiral cross-sectional phase.

Gaussian, Bessel, and Airy beams can be tailored to carry OAM by incorporating a spiral phase onto the existing beam profile, as shown in [22]. Various methodologies exist for generating OAM-carrying vortex beams, including the use of spiral phase plates, traveling-wave antennas, and circular antenna arrays. Among these, spiral phase plates are commonly employed, involving the passage of a Gaussian beam with a planar wavefront. These plates are crafted from a dielectric material with a varying spiral thickness, with the design of the step height of the spiral (h_t) formulated as

$$h_t = \lambda \frac{l}{\delta n}. \tag{23}$$

The parameter λ represents the design frequency, the symbol l denotes the desired mode of the resulting beam, and δn signifies the disparity between the refractive index of the dielectric plate and air. Consequently, the conventional Gaussian beam undergoes a transformation into a Laguerre–Gaussian (LG) beam. The amplitude distribution of the LG_l beam with mode l [3] is thereby determined by

$$LG_l(r,\theta,z) = E(r,z)\exp(jl\theta) \tag{24}$$

where the field distribution $E(r, z)$ delineates the Gaussian propagation in cylindrical coordinates from (10). Now, we place a specific concern on the additional phase acquired from the azimuthal index l.

The family of Bessel beams also demonstrates the potential to carry OAM. In this context, the beam profile $B(r,\theta,z)$ is defined as

$$B(r,\theta,z) = J_l(k_r r)\exp(jk_z z)\exp(jl\theta) \tag{25}$$

where the function $J_l(\cdot)$ denotes the Bessel function of l order. Once again, as in the discussion of Bessel beams, we recall that we are utilizing a cylindrical coordinate system because of the convenience of radial symmetry. Upon setting l to zero, denoting the absence of a topological charge, we return to the zeroth-order Bessel function, as already discussed. Consequently, the design and propagation principles therein are equally valid for higher order Bessel functions.

Irrespective of the underlying beam profile, an integer value of the topological charge l signifies an OAM beam as "pure." Pure OAM modes are mutually orthogonal, manifesting no crosstalk or interference, in theory. This is seen by the correlation between two OAM beams. Ignoring the amplitude components, we can observe that the correlation between the phases will be given as

$$\int_0^{2\pi} \exp(jl_1\theta)\exp(jl_2\theta)^* d\theta = \begin{cases} 0 & l_1 \neq l_2 \\ 2\pi & l_1 = l_2 \end{cases}. \tag{26}$$

Thus, if data streams have different OAM modes, we can enable their coexistence in the same frequency, time, and space channels without encountering interference. This introduces an additional layer of optimization for enhancing the system capacity [17]. OAM mode multiplexing has been demonstrated in both the optical and mm-Wave domains, where it is seen that the number of OAM modes is restricted by the design technique [24].

OAM multiplexing is also compared with classical MIMO systems. For a given antenna array size, it has been observed that the capacity achieved from OAM communications aligns with that of classical uncorrelated MIMO systems [25]. Nonetheless, OAM-based mode division multiplexing provides a more streamlined receiver architecture and higher capacity compared to point-to-point MIMO, especially in scenarios where MIMO systems demonstrate some level of correlation leading to a reduction in channel rank, which is particularly pronounced in THz-band signals [25].

Receiver performance and operation

Conventionally, a receiver can be designed independently of the transmitter. This is often expressed in the form of the link budget, where the received power P_{Rx} is calculated by following the Friis path loss equation:

$$P_{\text{Rx}} = P_{\text{Tx}} \frac{G_{\text{Tx}}\lambda^2}{(4\pi R)^2} G_{\text{Rx}} \tag{27}$$

where P_{Tx} is the transmitted power, $G_{\text{Tx}} = 4\pi A_{\text{eff}}/\lambda^2$ is the gain of the transmitter with an effective aperture area of A_{eff}, and G_{Rx} is the gain of the receiver antenna, with the transmitter and receiver separated by a distance R. The Friis path loss comes from far-field assumptions. Otherwise, the gain would continue to increase with an increasing aperture, leading to infinite gain of the antennas, which would result in deriving more received power than transmitted—a natural contradiction. Thus, in the near field, a more generalized link budget is formulated, given as [14]

$$\frac{P_{\text{Rx}}}{P_{\text{Tx}}} = \frac{\iint |E_2(x_2,y_2,z)|^2 dS_{\text{Rx}}}{\iint |E_1(x_1,y_1,0)|^2 dS_{\text{Tx}}} \tag{28}$$

where E_1 is the field at the emitter plane (at $z = 0$), E_2 is the field at the receiver plane, and where the integrals are performed over the receiver and transmitter apertures, S_{Rx} and S_{Tx}, respectively.

Thus, while utilizing wavefront engineering can make it possible to have more of the transmitted power incident on the receiver by truncating the decimating effects of the THz channel, ultimately, the receiver needs to be designed such that it is efficiently coupled to the characteristics of the incident electric field. This will allow us to obtain the maximum SNR possible, with perfect coherent coupling of the incident electric fields with the receiver. Recent studies, such as those in [14], assume such perfect coupling. However, as shown in [8], when nonuniform phases are present in the incident field, the receiver must then be able to accommodate the required delay-and-sum method for coherently adding such a nonuniform power profile [8].

For THz Bessel beams, the intensity pattern from the Bessel beams has a uniform phase, with the intensity being inconsistent. Thus, the total power from Bessel beams that is transmitted to the receiver is given as [2] $P_{\text{Rx}} = NP_T(1/(1+4M/3))$, where N is the number of rings that the receiver can intercept out of M total rings generated at the transmitter with total power P_T. With

THz Airy beams, the receiver should be tuned to be coherent toward the incident angle defined by the curve of the Airy beam (similar to the far-field beamsteering direction of arrival) [14].

When required to demultiplex multiple OAM modes, the receiver must employ a large enough aperture with a specific phase-based diffraction grating that exploits the principle of zero cross correlation in OAM modes for ease of demultiplexing [26]. Nonetheless, the fundamental principles remain the same; more power received coherently allows for greater SNR and performance metrics.

Applications in common THz issues

In this section, we discuss some of the latest applications that become possible with near-field cognizant wavefronts (see Figure 7). These applications are not exhaustive; however, they have been demonstrated at least partially with either simulation or experimental results. Thus, they form a strong first principles cornerstone in considering the possibilities with wavefront engineering in (sub-)THz links.

Increased energy efficiency and radiation gain

The energy cost of THz communications is still a significant challenge, primarily because of the lack of efficient THz radiation generation in comparison to power generation at lower frequencies. In addition to significant advances in device technology [1], wavefront engineering can also be a potential solution since the beam energy can be better focused toward the intended directions. The substantial energy challenge of blockages can be addressed by leveraging the self-healing and self-accelerating properties of Bessel and Airy beams. In addition, the actual received SNR can be drastically improved compared to utilizing simple near-field beamforming. One way to do so is through the aspect of the effective normalized radiation gain. Simply speaking, this involves determining that, if an additional wavelet or antenna element is added to the radiating sources, how effectively it superimposes the EM field. The maximum value is then 1, which indicates that all of the radiation from this additional source adds up coherently with the other fields. In [9] and [10], the normalized radiation gain under the application of Bessel beams, beamfocusing, and beamforming was presented. It was shown that, with beamforming, the normalized gain is notably crippled at even the limits of most indoor THz wireless local area networks (several tens of meters). In contrast, the near-field validity of Bessel beams and beamfocusing results in a significantly improved radiation gain for the same settings. The improvement in the receiver SNR with Bessel beams compared to beamforming is also experimentally validated in [7]. Simply speaking, a larger aperture allows more focused beams in beamfocusing—Bessel and Airy beams—as compared to the plane-wave Gaussian beams. Thus, the aspects of increasing radiation gain and energy efficiency with beamshaping in the near field are tremendous. All of this holds regardless of whether we utilize a singular large antenna, an array of subarrays, or a metasurface.

Minimizing the effect of blockage

The potential of wavefront engineering in mitigating the impact of obstacles to THz signal propagation has also been demonstrated in the literature. Specifically, Bessel beams are self-healing up to a significant aspect of blockage, and this property

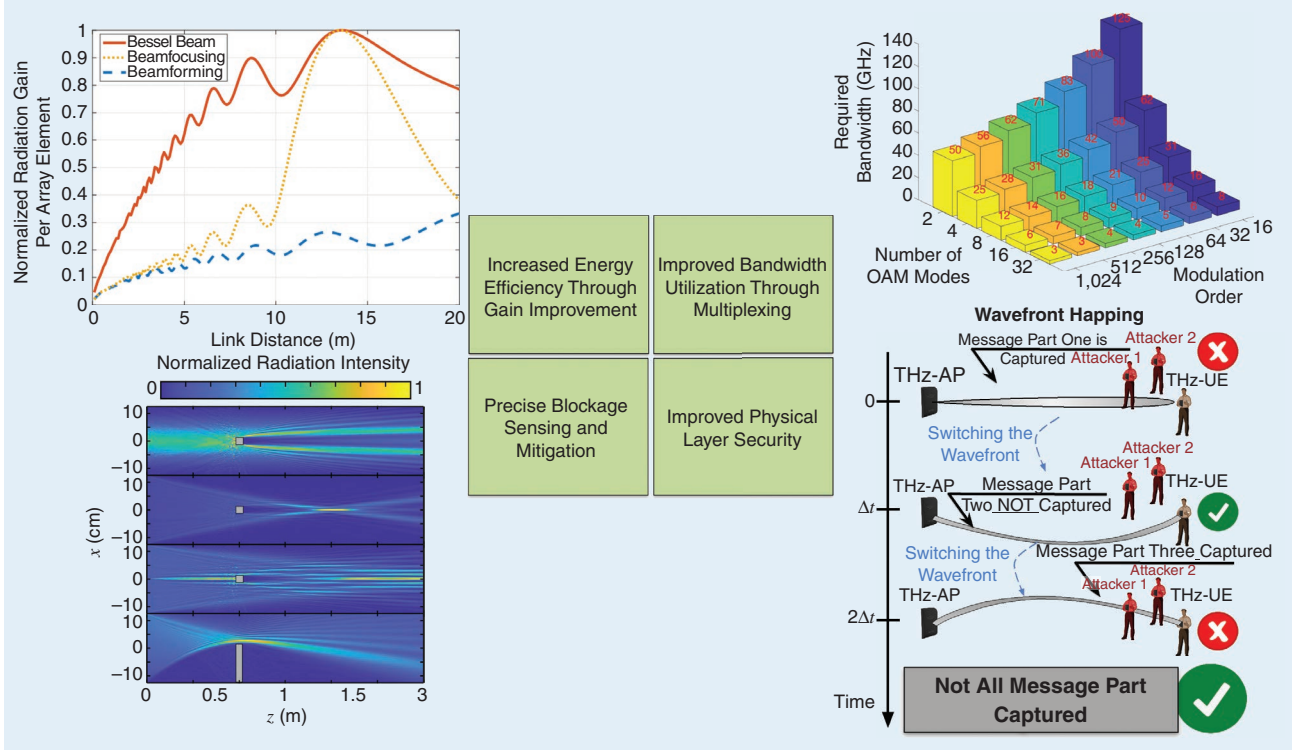

FIGURE 7. Demonstrated and proposed applications with THz near-field beams [7], [8], [9], [10], [14], [25], [27].

has been previously investigated in the mmWave and optical domains. More recently, in [7], we showed the self-healing nature of Bessel beams in ultrabroadband links at sub-THz frequencies. It was shown that, even with an obstruction blocking as much as 40% of the main radiating aperture, Bessel beams could provide up to 14 dB more SNR than beamforming, allowing for more than an order of magnitude improvement in the resultant bit error rate. The recent additional possibilities in blockage mitigation with THz Airy beams have been shown in [14], where it has been shown that Airy beams can facilitate blockage mitigation by completely curving around the blockage, thus providing more than 3 dB of gain in the near field.

With beamfocusing, the radiation from the portion of the aperture not blocked by the obstacle can still converge to focus at the desired focal point. However, this is not technically "self-healing," as the focal spot has not yet been formed; were the obstacle closer to the focal point, the blockage would be severe. By contrast, the self-healing nature of Bessel beams *reforms the beam* beyond the obstacle, and the performance of the Airy-like beam also remains impervious to the blockage since the beam can be designed to curve around this obstruction. Thus, Bessel and Airy beams seem more suitable for blockage reduction in THz near-field applications.

System capacity increase

The exploitation of wavefronts that carry OAM, such as higher order Bessel beams in the near field, allows the creation of perfect parallel orthogonal channels. This allows the creation of either 1) multiple space, time, and frequency channels separated by the modes of the OAM for a very high capacity link, perhaps ideally in the backhaul regime, or 2) the facilitation of multigigabit/second links with multiple modes that each utilize a small bandwidth, thus facilitating the benefits of very high connectivity at THz frequencies while still being relatively narrowband, relaxing the constraints of wideband issues in wavefront engineering. As shown in [25], OAM multiplexing can significantly improve the multiplexing capabilities in wireless systems, without an undue increase in the system complexity.

It is observed from [10] that the demand on the bandwidth as well as the requirement of higher order modulations can be significantly reduced when OAM multiplexing is utilized. In fact, the use of multiplexing via OAM becomes even more useful when we consider the fact that the maximum available consecutive bandwidth is limited in the THz band. This arises both from the limits of mixer technology and the presence of Earth exploration satellites (EESs) in the corresponding frequency range [28]. As an illustration, even the mixer unit incorporated in the 0.75 to 1.1-THz front ends by Virginia Diodes has a maximum limit of a 50-GHz bandwidth [29]. Consequently, there is a need for spectral efficiency in the order of tens of bits/second/hertz to satisfy the requirement of data rates of hundreds of gigabits/second or terabits/second with such an available bandwidth. Further yet, it is not trivial to utilize increasingly more bandwidth as that will be accompanied by a greater noise power [30], which curtails the feasibility of high-order modulation schemes. Alternatively, for example, 32 distinct OAM beams can help sustain a 1-Tb/s link with a bandwidth of less than 10 GHz, even if 16-quadrature amplitude modulation is utilized [10]. Hence, in the presence of a sufficiently high SNR, OAM multiplexing can effectively replace or complement THz MIMO, thus relaxing the bandwidth requirements for the desired data rate. The latter could also facilitate the spectrum utilization and the coexistence of prospective THz links with other services (e.g., EESs).

Physical layer security

Physical layer security continues to play a crucial role in the concerns for 6G networks. As quantum communications continue to arise, conventional cryptography methods cannot be utilized to ensure protection from eavesdropping and jamming attacks. Here, wavefront engineering again provides an opportunity. More specifically, it has previously been shown that even directional beams can be eavesdropped by placing a small obstruction in the path of the beam, creating a secondary link to an eavesdropper [1]. At the same time, the work in [31] has shown that it becomes possible to take a message signal $m(t)$, and split it into two or more parts $s_1(t), s_2(t) \ldots . s_N(t)$ through a code such that successful eavesdropping is possible only when all of the individual parts are recovered. Motivated by this, in [27], we recently proposed the concept of utilizing wavefront switching. Here, Airy beams with different curvatures and also Bessel beams can all be utilized to carry the individual components of a message, following spatially different paths from the transmitter to the receiver, even without any additional resources, such as smart RISs. This allows us to drastically reduce the spatial region where common subsets of the message code can be eavesdropped, except in very close proximity to the receiver. Indeed, we have shown that as long as a 1.5-m area can be secured around the receiver, absolute secrecy can be guaranteed. This clearly opens the door for novel physical layer security features. Perhaps best of all, the technique of utilizing different wavefronts in no way stops the application layer cryptography or cybersecurity measures, thus making the two techniques complementary to each other.

Research challenges and opportunities

The efficient harnessing of novel wavefronts and their attractive properties within widespread 6G and beyond scenarios is a wide research area with many open challenges, which are summarized in Figure 8.

Choosing the beamshape in the near field

The overarching scope of this tutorial shows that diverse beamshapes exist in the near field. Their choice can be decided by considering the specific applications that they can achieve, as provided in the previous section. Perhaps most importantly, the 1D counterparts of these beams can also be investigated as candidate wavefronts in the near field. Essentially, while the existence of all of the beams is clear, and the common thread in here is the design of the wavefront, the exact candidate beamshape, or a combination of these for 6G (sub-)THz wireless, still needs to be decided upon.

Generating wavefronts in practice

Each beamshape has a corresponding wavefront; thus, generating a specific beam is essentially the task of generating the specific wavefront. At a preliminary glance, we see that wavefronts are generated only by changing the phase across the radiating aperture, which can be through phase shifters in traditional antenna arrays, or lenses. At the same time, exploiting RISs and metasurface antennas is also possible. Holographic beamforming has also been proposed for next-generation wireless, where the power consumption is drastically reduced and the size of the arrays can be scaled significantly [16]. Nonetheless, the development of arrays that can provide the same gain and beam design as commercially available lens and reflector systems is still challenging since the requisite array at these frequencies would need many thousands of elements.

Lenses from dielectric materials provide continuous precise wavefronts, but they lack reconfigurability—an obvious limitation for serving dynamic beams. In other setups with arrays or wavelets, a simple limitation in the "purity" of the generated beam is the discretized phase. Essentially, when utilizing conventional antenna elements with present phase shifters that have a limited discretized phase response, the spatial resolution and phase resolution of the aperture are decreased [16]. Utilizing a metasurface approach with subwavelength radiating elements could increase the spatial resolution [16]. Nonetheless, metasurfaces must be controlled globally since the radiation response is tightly coupled across all of the subwavelength elements, making their operation more complex.

However, reconfigurable arrays and metasurfaces are being developed for 6G and beyond—for example, with new proposed physics, such as graphene plasmonics [32]—whereby it appears that dynamic and advanced beamshaping through wavefront engineering will be possible in the 6G and beyond landscape. In [13], it has been shown that, if practical phase shifters can accommodate a $\pi/8$-radian phase shift (4-bit resolution), then most beamshaping paradigms can be sufficiently applied. Thus, this becomes a lower threshold to aim for in integrated chip (IC) and chip design. The ambitious task of generating these beams has already spurred initial results, and more robust arrays are in development [23]. Thus, while present-day experiments may still utilize lenses to validate the principles of these beams, more dynamic configurations are up-and-coming.

Near-field channel modeling

Until recently, near-field channel modeling has been mostly theoretical, employing the spherical-wave model for beamfocusing only [8]. Our preliminary experimental work shows that the near-field THz channel cannot be agnostic of the antenna, at least when Gaussian beams are utilized [11]. All of this clearly indicates that a better understanding of the comprehensive near-field THz channel itself is required as an immediate next step. One method would be to engage in comprehensive and exhaustive solutions of Maxwell's equations for all possible beamshapes in multiple specific scenarios. However, this isn't always possible, and it would have a prohibitive computational and validation time. Recently, machine learning-based neural networks have been proposed that have a physics-aware loss function. These solvers are proposed to help in developing THz-specific channel models or approximations for near-field propagation in target setups, such as indoor and outdoor wireless access.

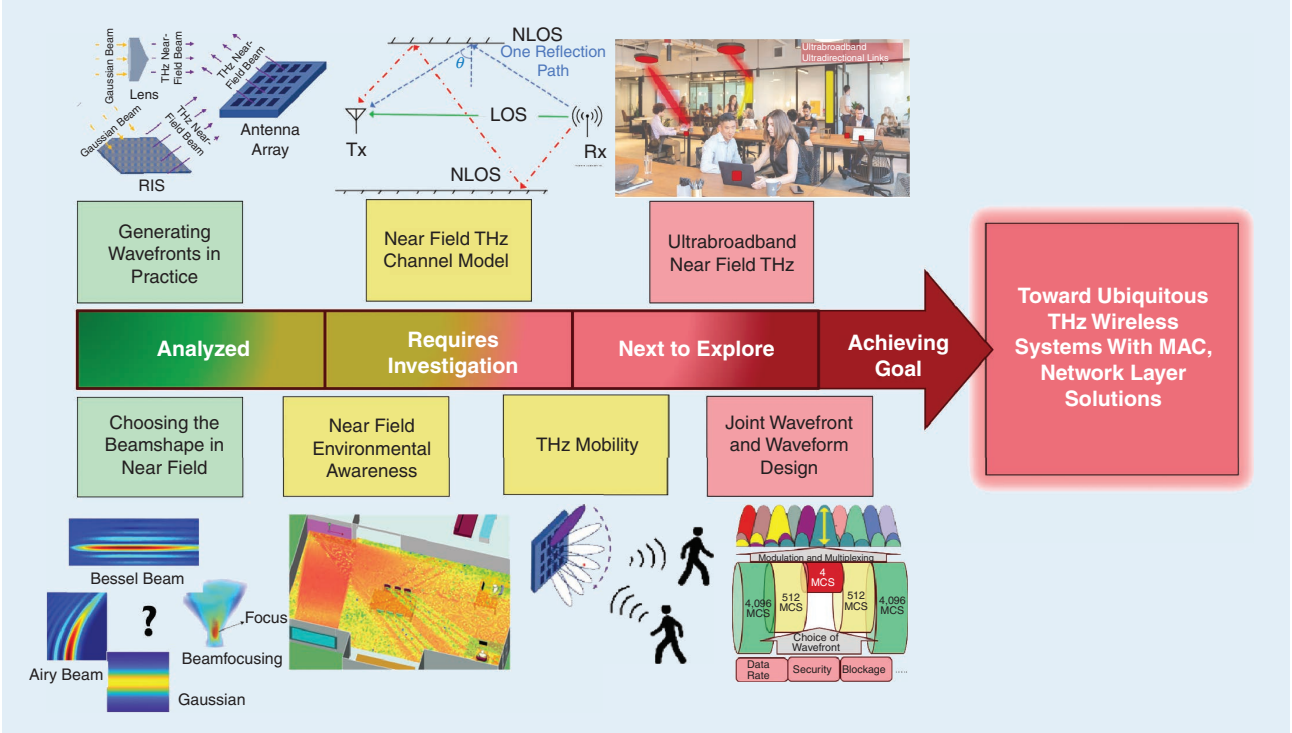

FIGURE 8. Engineering challenges and opportunities within the near field of THz communications. MAC: media access control; MCS: modulation and coding scheme.

By testing more straightforward predictions in these solvers and verifying with experimental characterizations, the numerical solvers can also be partially validated. These solvers could then be utilized in predicting channel response in multiple situations and ultimately lead to the development of channel models where the equivalent near-field path loss can be accounted for. In addition, with scattering and reflections more likely to be nontrivial within the near field, the Rician factor and delay spread profiles should also be determined.

Near-field environmental awareness

Joint communication and sensing is today considered an important aspect of possible use cases with THz. The idea is to utilize the same waveform for communications while also obtaining localization information that can be beneficial. This highlights how important localization is in the 6G landscape since, with environmental awareness, dynamic links can be generated, their paths can be predicted, and spectrum use can be improved [1]. It is worth noting that the discussed beamshapes have been heavily investigated first in sensing and imaging applications within the optical domain. Thus, in THz imaging and sensing, investigating the applicability and impact of beamshaping can play a crucial role in the sensing capabilities of next-generation networks. For example, the higher gain from beamshaping with Bessel beams can allow for greater noise tolerance, increasing the bandwidth that can be incorporated within the system without sacrificing the SNR required for precise sensing. At the same time, however, near-field sensing can also help in detecting blockage, which could affect the design and control of Bessel and Airy beams. However, it is interesting to note that the radar cross section is a far-field parameter, and thus, it isn't trivial to characterize blockages or objects in the near field. Some early investigations on near-field radar cross section (RCS) equivalence are presented in [33]. This was done only for the spherical model of beamfocusing, and whether these models can be extended to near-field Bessel and Airy beams remains an area of investigation.

An interesting direction here is to investigate whether the spatial Fourier transform between the near and far fields can also be extended to the RCS derivations. Overall, a general model to help capture the complexity of these beams for designing near-field sensing capabilities is a promising research avenue.

Mobility in near-field THz

All of the beam types that we have discussed in the section "Near-Field THz Beams" have been discussed for the broadside case. However, it is possible to generate these beams in other directions and, in the case of beamfocusing, focus on different points. However, there are significant challenges that come into play here. First, as soon as we add a steering phase, we see the issue of beamsquint in beamforming, and we can expect to see similar issues in Bessel beams that are steered off axis. Second, when we steer away from the broadside, we notice that the effective size of the aperture is reduced, as also highlighted in [8], due to which the near-field effect can be changed, thus changing the distance up to which these near-field beams will be generated. In part, this is why we advocate for beamswitching mechanisms [27] since it seems unlikely that a single type of beam can satisfy all of the constraints of near-field THz wireless. We need to first explore the works of steering of Bessel beams, which have been recently discussed in [34], and observe the changes to the maximum propagation distance as well as the suitable bandwidth in the absence of true-time delay (TTD) lines. Also, with Airy beams having been very recently demonstrated, we note that the task on steering these beams is only just getting started. Here, we must develop a method to evaluate how often we need to recalculate the desired trajectory such that steering is enabled, and how much this will increase the design complexity. The design of apertures which can enable steering of such exotic beams may require a different design approach, as highlighted in [34].

Ultrabroadband near-field THz

Broadband communications are considered a fundamental aspect of THz systems—it does little to achieve connectivity at these frequencies without high system capacity. However, wavefront engineering is a narrowband technique: a feature of a beam may not extend uniformly across a large bandwidth as the same phase delay does not generate the same time delay that truly governs wave propagation, superposition, and final beamshape. TTD lines can be utilized to counter this problem through a frequency-dependent phase profile that makes the time delay uniform. However, the required architecture is more complex [13].

Narrowband phase shifters are more likely, where the performance of a particular beam is dependent on the bandwidth, as explained in the section "Near-Field THz Beams." At the same time, utilizing OAM to enable multimode multiplexing is one way in which a smaller bandwidth can be utilized without reducing the desired system capacity. In fact, since OAM multiplexing/demultiplexing is less demanding from a signal processing perspective compared to THz MIMO, and because THz MIMO is already inefficient because of highly correlated sparse channels, this could be a promising research direction to explore. Nonetheless, if the bandwidth within the OAM mode is large enough, or the OAM modes are steered away from the broadside, the generated OAM modes have a spillover effect and become impure, causing interference with other OAM modes [25]. Thus, critical investigations and unbiased evaluations of OAM versus other spatial multiplexing methods are needed to properly characterize these new performance–complexity tradeoffs.

At the same time, a sufficiently complex transmitter could simultaneously generate a multiwavefront beam for a massive system capacity: imagine a transmitter that focuses a beam for some users, creates a Bessel beam for some other users, and also connects to other users through curving Airy beams. All of this would require extremely complicated numerical simulations and EM computations to first arrive at an array design, followed by cutting-edge IC design to fabricate the array, and further yet innovative mechanisms to test and benchmark the performance of the device.

Joint wavefront and waveform design

Wavefront engineering and utilization are independent of the underlying waveform design as long as the bandwidth is provided (either with OAM or TTD lines). Across a larger bandwidth, we can account for distortions and preequalize for them within the waveform design. The meticulous design of waveforms is thus pivotal in ensuring link reliability through adaptive techniques that address the dynamic nature of the channel. On the one hand, leveraging different wavefronts could bolster the link quality by enhancing SNR, mitigating blockages, and fortifying security. On the other hand, the judicious selection of waveforms can allow for maximum exploitation of these factors, while also correcting for distortions introduced from bandwidth limits of the wavefront. In addition, when the near field can manifest in extremely important channel characteristics and metrics including path loss, *K*-factor, and delay spread, this automatically makes it critical in deciding on the choice of the waveform [11]. Further, it is imperative to account for underlying device limitations, like phase noise and peak-to-average power constraints [30], in the wavefront design. Thus, a unified approach integrating wavefront and waveform design embodies critical significance, particularly in the context of sub-THz and THz near-field communication.

Toward ubiquitous wireless

The aforementioned challenges can help to tackle the physical layer design in near-field THz. However, more pressing issues open for the media access control (MAC) and networking layers. For example, when considering MAC design, interference modeling plays a crucial role [35]. However, all of these studies utilized plane-wave assumptions, and thus need to be revisited for more exotic beamshapes.

Further yet, beamswitching through the principle of wavefront hopping has been recently proposed. This can lead to high gains in physical layer security, interference mitigation, and spectrum reuse [27]. Beamshaping also challenges conventional networking solutions: Should THz multiconnectivity be explored to the level at which it was considered necessary when only beamforming was a candidate beam profile? Or now, with the prospect of realizing blockage-reliant and NLOS-capable links through, for example, Bessel and Airy beams, do the wireless nodes need to have other networking principles be put under consideration? All of these questions must be answered once the first crucial steps in the direction of THz wireless in the near field are satisfactorily addressed.

Conclusions

With continuous growth in user demands, the THz band is being explored for both high-rate data exchange and high-precision sensing in next-generation wireless systems. While massive strides have been made to conquer the THz band by conquering the THz-technology gap, a new issue has emerged in that canonical propagation principles from legacy RF systems cannot hold in the THz band. The THz physical layer must have a symbiosis of communication and wave theory, adopting the principles from optics to solve the pressing issues of RF. This challenge, however, simultaneously offers us a Goldilocks zone, where beams that have previously never been considered in cellular wireless and that provide untapped applications and opportunities can become readily utilizable to facilitate ultrabroadband communications. The design of these beams is dependent on their underlying wavefront, and by exploiting the features of these wavefronts, one can realize efficient and practical THz communication systems that can constitute an inherent part of the 6G and beyond landscape. Several foundational principles and demonstrations that validate this exciting research direction have been demonstrated. However, the full realization of near-field THz wireless is still on the horizon. Addressing the underlying research challenges can and must become a key goal of enabling THz communications, which has the potential to revolutionize the wireless landscape.

Acknowledgment

This work was supported in part by U.S. Air Force Office of Scientific Research Grant FA9550-23-1-0254 and in part by U.S. National Science Foundation Grants CNS-2225590 and CNS-1955004. V. Petrov acknowledges the support from Digital Futures at KTH, Stockholm, Sweden, and Grant 2022–04222 from the Swedish Research Council. A. Singh and P. Sen are supported by Air Force Research Laboratory Grant FA8750-22-2-0500 (subaward 141496 - 23166) as well as the WINGS Center for Excellence at the State University of New York Polytechnic Institute.

Authors

Arjun Singh (singha8@sunypoly.edu) received his Ph.D. degree in electrical engineering from Northeastern University, Boston, USA, in 2021. He is an assistant professor in the Electrical and Computer Engineering Program at the State University of New York Polytechnic Institute, Utica, NY 13504 USA, where he also serves as the director of the Wireless and Intelligent Next Generation Systems Center. His research interests include realizing terahertz-band wireless communications for 6G and beyond. In this area, he has coauthored more than 15 journals, 26 conferences, and two U.S. patents. He is a Member of IEEE.

Vitaly Petrov (vitalyp@kth.se) received his Ph.D. degree in communications engineering from Tampere University, Finland, in 2020. He is an assistant professor with the Division of Communication Systems and Digital Futures, KTH Royal Institute of Technology, 114 28 Stockholm, Sweden. Before joining KTH in 2024, he was a principal research scientist at Northeastern University, Boston, MA, USA (2022–2024) and a senior standardization specialist and a 3GPP RAN1 delegate with Nokia Bell Labs and later Nokia Standards (2020–2022). His research interests include near-field terahertz band communications and networking. He is a Member of IEEE.

Priyangshu Sen (senp@sunypoly.edu) received his Ph.D. degree from Northeastern University, Boston, MA, USA, in 2022. He is an assistant professor in the Engineering Department at State University of New York Polytechnic Institute, Utica, NY 13504 USA. He was a wireless system development engineer at Amazon in the United States from

2022 to 2023. His research interests include experimental and statistical characterization of terahertz (THz) communication channels and networks. He has coauthored two book chapters, 10 journal articles, and 12 conference papers in THz communications. He is a Member of IEEE, the EDAS chair for the 2025 IEEE Consumer Communications & Networking Conference, and was chair of the Workshop on Terahertz Communications, Sensing, and Security at the 2024 IEEE Military Communications Conference.

Josep Miquel Jornet (jmjornet@northeastern.edu) received his Ph.D. degree in electrical and computer engineering from the Georgia Institute of Technology in 2013. He is a professor in the Department of Electrical and Computer Engineering at Northeastern University (NU), Boston, MA 02115-5026 USA, the associate director of the Institute for the Wireless Internet of Things at NU, and the director of the Ultrabroadband Nanonetworking Laboratory. His research interests are in terahertz communication networks and wireless nano–bio–communication networks. He is a Fellow of IEEE, an IEEE ComSoc Distinguished Lecturer (class of 2022–2024), editor-in-chief of Elsevier's *Nano Communication Networks*, and an editor of *IEEE Transactions on Communications*.

References

[1] I. F. Akyildiz, C. Han, Z. Hu, S. Nie, and J. M. Jornet, "Terahertz band communication: An old problem revisited and research directions for the next decade," *IEEE Trans. Commun.*, vol. 70, no. 6, pp. 4250–4285, Jun. 2022, doi: 10.1109/TCOMM.2022.3171800.

[2] J. Durnin, J. Miceli, and J. H. Eberly, "Comparison of Bessel and Gaussian beams," *Opt. Lett.*, vol. 13, no. 2, pp. 79–80, Feb. 1988, doi: 10.1364/OL.13.000079.

[3] L. Allen, M. W. Beijersbergen, R. J. C. Spreeuw, and J. P. Woerdman, "Orbital angular momentum of light and the transformation of Laguerre-Gaussian laser modes," *Phys. Rev. A*, vol. 45, no. 11, Jun. 1992, Art. no. 8185, doi: 10.1103/PhysRevA.45.8185.

[4] J. Durnin, "Exact solutions for nondiffracting beams. I. The scalar theory," *J. Opt. Soc. Amer. A*, vol. 4, no. 4, pp. 651–654, Apr. 1987, doi: 10.1364/JOSAA.4.000651.

[5] G. Siviloglou, J. Broky, A. Dogariu, and D. N. Christodoulides, "Observation of accelerating Airy beams," *Phys. Rev. Lett.*, vol. 99, no. 21, Nov. 2007, Art. no. 213901.

[6] A. Bhattacharyya, J. M. Merlo, S. R. Mghabghab, A. Schlegel, and J. A. Nanzer, "Multiobjective distributed array beamforming in the near field using wireless syntonization," *IEEE Microw. Wireless Technol. Lett.*, vol. 33, no. 6, pp. 775–778, Jun. 2023, doi: 10.1109/LMWT.2022.3231183.

[7] I. V. Reddy, D. Bodet, A. Singh, V. Petrov, C. Liberale, and J. M. Jornet, "Ultrabroadband terahertz-band communications with self-healing Bessel beams," *Commun. Eng.*, vol. 2, no. 1, 2023, Art. no. 70, doi: 10.1038/s44172-023-00118-8.

[8] M. Cui, Z. Wu, Y. Lu, X. Wei, and L. Dai, "Near-field MIMO communications for 6G: Fundamentals, challenges, potentials, and future directions," *IEEE Commun. Mag.*, vol. 61, no. 1, pp. 40–46, Jan. 2023, doi: 10.1109/MCOM.004.2200136.

[9] K. Dovelos, S. D. Assimonis, H. Q. Ngo, B. Bellalta, and M. Matthaiou, "Intelligent reflecting surfaces at terahertz bands: Channel modeling and analysis," in *Proc. IEEE Int. Conf. Commun. Workshops (ICC Workshops)*, Piscataway, NJ, USA: IEEE Press, 2021, pp. 1–6, doi: 10.1109/ICCWorkshops50388.2021.9473890.

[10] A. Singh et al., "Wavefront engineering: Realizing efficient terahertz band communications in 6G and beyond," *IEEE Wireless Commun.*, vol. 31, no. 3, pp. 133–139, Jun. 2024, doi: 10.1109/MWC.019.2200583.

[11] P. Sen, S. Badran, V. Petrov, A. Singh, and J. M. Jornet, "Impact of the antenna on the sub-Terahertz indoor channel characteristics: An experimental approach," in *Proc. IEEE Int. Conf. Commun. (ICC)*, 2024, pp. 2537–2542, doi: 10.1109/ICC51166.2024.10622180.

[12] C. A. Balanis, *Antenna Theory: Analysis and Design*. Hoboken, NJ, USA: Wiley, 2016.

[13] D. Headland, Y. Monnai, D. Abbott, C, Fumeaux, and W. Withayachumnankul, "Tutorial: Terahertz beamforming, from concepts to realizations," *APL Photon.*, vol. 3, no. 5, Feb. 2018, Art. no. 051101, doi: 10.1063/1.5011063.

[14] H. Guerboukha, B. Zhao, E. Knightly, and D. M. Mittleman, "Curving THz wireless data links around obstacles," *Commun. Eng.*, vol. 3, no. 1, 2024, Art. no. 58, doi: 10.1038/s44172-024-00206-3.

[15] C. Han, L. Yan, and J. Yuan, "Hybrid beamforming for terahertz wireless communications: Challenges, architectures, and open problems," *IEEE Wireless Commun.*, vol. 28, no. 4, pp. 198–204, Aug. 2021, doi: 10.1109/MWC.001.2000458.

[16] M. D. Renzo et al., "Smart radio environments empowered by reconfigurable AI meta-surfaces: An idea whose time has come," *EURASIP J. Wireless Commun. Netw.*, vol. 2019, no. 1, pp. 1–20, May 2019.

[17] H. Zhou et al., "Utilizing multiplexing of structured THz beams carrying orbital-angular-momentum for high-capacity communications," *Opt. Express*, vol. 30, no. 14, pp. 25,418–25,432, Jun. 2022, doi: 10.1364/OE.459720.

[18] F. Depasse, M. Paesler, D. Courjon, and J. Vigoureux, "Huygens–Fresnel principle in the near field," *Opt. Lett.*, vol. 20, no. 3, pp. 234–236, 1995, doi: 10.1364/OL.20.000234.

[19] V. Petrov, J. M. Jornet, and A. Singh, "Near-field 6G networks: Why mobile terahertz communications MUST operate in the near field," in *Proc. IEEE Global Commun. Conf. (GLOBECOM)*, 2023, pp. 3983–3989, doi: 10.1109/GLOBECOM54140.2023.10436942.

[20] "Gaussian beam propagation," Edmund Optics. Accessed: Jun. 24, 2024. [Online]. Available: https://www.edmundoptics.com/knowledge-center/application-notes/lasers/gaussian-beam-propagation/

[21] S. N. Khonina, N. L. Kazanskiy, S. V. Karpeev, and M. A. Butt, "Bessel beam: Significance and applications—A progressive review," *Micromachines*, vol. 11, no. 11, 2020, Art. no. 997, doi: 10.3390/mi11110997.

[22] S. Li and J. Wang, "Adaptive free-space optical communications through turbulence using self-healing Bessel beams," *Sci. Rep.*, vol. 7, no. 1, pp. 1–8, Feb. 2017, doi: 10.1038/srep43233.

[23] S. Venkatesh, X. Lu, H. Saeidi, and K. Sengupta, "A high-speed programmable and scalable terahertz holographic metasurface based on tiled CMOS chips," *Nature Electron.*, vol. 3, no. 12, pp. 1–9, 2020, doi: 10.1038/s41928-020-00497-2.

[24] G. Ruffato, M. Massari, and F. Romanato, "Multiplication and division of the orbital angular momentum of light with diffractive transformation optics," *Light: Sci. Appl.*, vol. 8, no. 1, pp. 1–13, 2019, doi: 10.1038/s41377-019-0222-2.

[25] H. Zhao, B. Quan, X. Wang, C. Gu, J. Li, and Y. Zhang, "Demonstration of orbital angular momentum multiplexing and demultiplexing based on a metasurface in the terahertz band," *ACS Photon.*, vol. 5, no. 5, pp. 1726–1732, 2017, doi: 10.1021/acsphotonics.7b01149.

[26] V. Petrov, D. Bodet, and A. Singh, "Mobile near-field terahertz communications for 6G and 7G networks: Research challenges," *Frontiers Commun. Netw.*, vol. 4, Mar. 2023, Art. no. 1151324, doi: 10.3389/frcmn.2023.1151324.

[27] V. Petrov, H. Guerboukha, D. M. Mittleman, and A. Singh, "Wavefront hopping: An enabler for reliable and secure near field terahertz communications in 6G and beyond," *IEEE Wireless Commun.*, vol. 31, no. 1, pp. 48–55, Feb. 2024, doi: 10.1109/MWC.003.2300310.

[28] C. Bosso, P. Sen, X. Cantos-Roman, C. Parisi, N. Thawdar, and J. M. Jornet, "Ultrabroadband spread spectrum techniques for secure dynamic spectrum sharing above 100 ghz between active and passive users," in *Proc. IEEE Int. Symp. Dyn. Spectr. Access Netw. (DySPAN)*, Piscataway, NJ, USA: IEEE Press, 2021, pp. 45–52, doi: 10.1109/DySPAN53946.2021.9677346.

[29] P. Sen, D. A. Pados, S. N. Batalama, E. Einarsson, J. P. Bird, and J. M. Jornet, "The TeraNova platform: An integrated testbed for ultra-broadband wireless communications at true terahertz frequencies," *Comput. Netw.*, vol. 179, Oct. 2020, Art. no. 107370, doi: 10.1016/j.comnet.2020.107370.

[30] P. Sen, V. Ariyarathna, and J. M. Jornet, "An optimized M-ary amplitude phase shift keying scheme for ultrabroadband terahertz communication," in *Proc. IEEE 19th Annu. Consum. Commun. Netw. Conf. (CCNC)*, Piscataway, NJ, USA: IEEE Press, 2022, pp. 661–666, doi: 10.1109/CCNC49033.2022.9700581.

[31] A. Cohen et al., "Absolute security in terahertz wireless links," *IEEE J. Sel. Topics Signal Process.*, vol. 17, no. 4, pp. 819–833, Jul. 2023, doi: 10.1109/JSTSP.2023.3307906.

[32] A. Singh, M. Andrello, N. Thawdar, and J. M. Jornet, "Design and operation of a graphene-based plasmonic nano-antenna array for communication in the terahertz band," *IEEE J. Sel. Areas Commun.*, vol. 38, no. 9, pp. 2104–2117, Sep. 2020, doi: 10.1109/JSAC.2020.3000881.

[33] T. Dogaru, "Near-field target scattering characterization and radar modeling," US Army Combat Capabilities Development Command, Army Research Laboratory, Adelphi, MD, USA, Tech. Rep., May 2021. [Online]. Available: https://apps.dtic.mil/sti/trecms/pdf/AD1132181.pdf

[34] G.-B. Wu, K. F. Chan, S.-W. Qu, and C. H. Chan, "A 2-D beam-scanning Bessel launcher for terahertz applications," *IEEE Trans. Antennas Propag.*, vol. 68, no. 8, pp. 5893–5903, Aug. 2020, doi: 10.1109/TAP.2020.2988936.

[35] H. Shokri-Ghadikolaei, C. Fischione, and E. Modiano, "Interference model similarity index and its applications to millimeter-wave networks," *IEEE Trans. Wireless Commun.*, vol. 17, no. 1, pp. 71–85, Jan. 2018, doi: 10.1109/TWC.2017.2762667.